Exploring alternative designs for a computational hyperspectral imager for microscopy

Yashovardhan Raniwala

Electrical Engineering and Computer Sciences
University of California, Berkeley

Technical Report No. UCB/EECS-2023-82
http://www2.eecs.berkeley.edu/Pubs/TechRpts/2023/EECS-2023-82.html

May 10, 2023

Exploring alternative designs for a computational hyperspectral imager for microscopy

by

Yashoavrdhan Raniwala

A thesis submitted in partial satisfaction of the

requirements for the degree of

Master of Science

in

Electrical Engineering and Computer Science

in the

Graduate Division

of the

University of California, Berkeley

Committee in charge:

Professor Laura Waller, Co-chair
Professor Michael Lustig, Co-chair

Spring 2023

The thesis of Yashoavrdhan Raniwala, titled Exploring alternative designs for a computational hyperspectral imager for microscopy, is approved:

Co-chair Laura Waller Date 5/9/23

Co-chair Miki Lustig Date 5/9/23

Date

University of California, Berkeley

Exploring alternative designs for a computational hyperspectral imager for microscopy

Abstract

Exploring alternative designs for a computational hyperspectral imager for microscopy

by

Yashoavrdhan Raniwala

Master of Science in Electrical Engineering and Computer Science

University of California, Berkeley

Professor Laura Waller, Co-chair

Professor Michael Lustig, Co-chair

Hyperspectral imaging (HSI) is an imaging technique that captures the spectral response for every point in the scene. It has application is remote sensing, agriculture, medical imaging, and fluorescence microscopy. A number of these applications require a snapshot HSI system with high acquisition speeds. However, most of these snapshot systems are either too bulky and expensive, or they require a custom fabrication process. This results in reduced accessibility to these systems due to price, long lead times, and lack of access to custom fabrication tools. We use a compact snapshot HSI system (Spectral Diffuserscope) as a reference to propose alternative designs that are simpler to reproduce.

In this work we present two designs for computational snapshot HSI systems which are simple to fabricate. They can both be fabricated in lab using mostly off-the-shelf components. This makes the system easier to reproduce and allows us to use an imaging sensor of our choice as part of our HSI system.

For the first design, we outline a detailed fabrication and calibration procedure. Additionally, we discuss appropriate computational modifications to improve reconstruction fidelity. We show initial experimental results to show how these modifications help improve reconstructions. We also discuss how to adapt the system for coupling into a benchtop microscope.

For the second design, we again outline a detailed fabrication and calibration procedure. We present initial simulation results to aid the design process if the system were to be fabricated. We briefly discuss the important design tradeoffs associated with this system and the possibilities of extending this work in the future.

To my family

I dedicate my research to my parents, who have always believed in me and supported me in every way possible. Their unwavering love and encouragement have been a constant source of inspiration for me. They believed in me in times when I doubted myself and have made efforts above and beyond to ensure I can achieve my potential. I also dedicate my research to my younger brother, whose passion for science exceeds that of my own. He constantly pushes me to be better than the limits I set for myself. Thank you for being there for me through the highs and lows. This research would not have been possible without their love, support, and encouragement.

Thank you to all who have supported me along the way, and to everyone who has contributed to my growth as a researcher and as a person.

Contents

List of Figures

Acknowledgments

Scientific advancement is rarely a product of individual brilliance, it takes a great community to bring ideas to fruition. First and foremost, I would like to express my deep appreciation to my research mentor, Neerja Aggarwal, and my advisor, Professor Laura Waller. Their guidance, support, and expertise have been invaluable to me throughout my research journey. I am grateful for their encouragement, feedback, and patience as I navigated through various challenges.

I want to especially recognize the impact that Neerja Aggarwal has had on me not just as an engineer but as a human being. She invests a lot of time in her mentees to help grow personally and professionally. She has made me a more confident learner and presenter, and has taught me the art of experimental research. I am grateful to you for being patient with my mistakes and taking the time make sure I can achieve my best. I am really inspired by her dedication towards perfecting applicable scientific research.

I would also like to thank Eric Markley and KC Lee for their assistance with my projects. Their expertise have been instrumental in helping me achieve my research goals. I am grateful for their willingness to share their knowledge and expertise, and for their support throughout my research. I extend my heartfelt thanks to the members of the Waller Lab for their insights and perspectives, which have made my research experience truly enjoyable and memorable.

Finally, I would like to express my gratitude to my family and friends for their love, support, and encouragement. Their unwavering belief in me has been a source of strength and motivation throughout my academic journey.

Chapter 1

Introduction

1.1 Overview

Hyperspectral Imaging (HSI)

Hyperspectral Imaging is an imaging technique that captures a high-resolution spectrum for each spatial point in an image. It has its origins in remote sensing and was developed over the late 1900s [15]. With advancements in computing power and spectral imaging technology, it became possible to develop sophisticated HSI sensors. As HSI technologies continued to advance, these systems have became much more compact and accessible for a variety of applications. The datacube captured in this technique is often called the hypercube and it consists of the usual spatial dimensions of the image and an additional wavelength dimension.

Applications of HSI

Since its inception, HSI technology has advanced and current HSI systems have been able to achieve much better image quality with much better form factor. Consequently, HSI has become a valuable tool for a variety of applications ranging from remote sensing to medical imaging. It is used for mapping and monitoring of land use, vegetation, and mineral resources [22]. HSI also has potential applications in medical imaging [20], for instance cancer diagnosis and monitoring [3]. Other applications include environmental monitoring [27], food quality control [16], agriculture [19], geology [26], forestry [1], and art conservation [18]. HSI also has important application in fluorescence microscopy including multi-label cell imaging [10] and spectrally coded beads for bio-assays [25] [14].

HSI Systems

HSI systems can be broadly classified into scanning based systems and snapshot systems. Scanning systems themselves are classified into spatial scanning systems and spectral scanning systems. As the name suggests, spatial scanning based systems acquire data by scanning

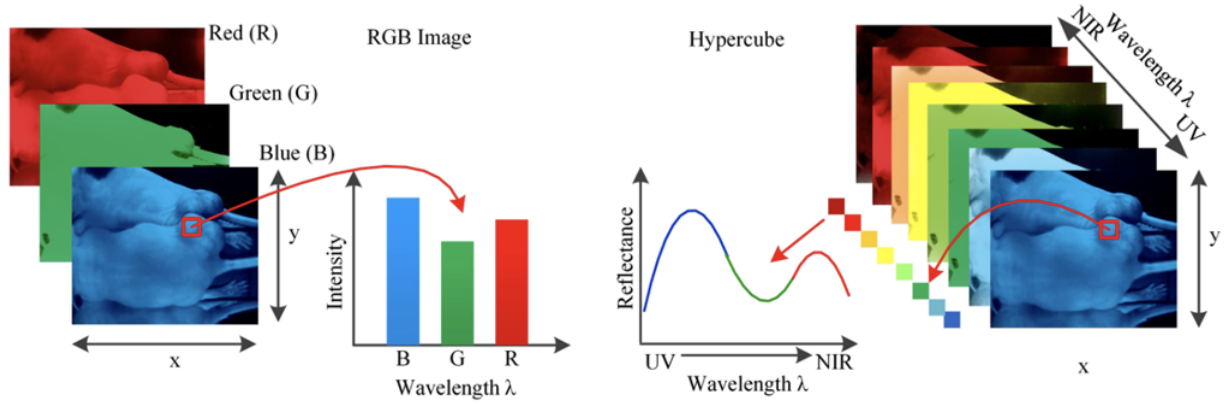

Figure 1.1: A conventional color image has 3 spectral channels, i.e., each pixel has 3 intensities associated with it, corresponding to red, green and blue colors (on the left). A hyperspectral image captures the intensity for every pixel across a range of wavelengths with high spectral resolution (on the right), giving both spatial and spectral information contained in the scene. Figure taken from [20]

through the scene with a sensor that captures all the spectral information at every point (or line). Analogously, spectral scanning systems capture the entire scene for a particular spectral band and scan through all the desired spectral bands to capture the hypercube. Such systems can achieve high spatial and spectral resolution but cannot be used in applications that require high temporal resolution (for example imaging dynamic scenes). Figure 1.2 and 1.3 show common architectures for such HSI systems.

Snapshot HSI systems capture the hyperspectral data of a scene in a single acquisition. These systems typically have lower spatial-spectral resolution than the scanning based systems so are mainly useful for dynamic scenes and applications that require high acquisition speeds. However, these systems are often bulky, expensive, have a number of additional components, and are hard to couple into existing bench-top microscopes [28] [30]. Some examples of such systems are shown in Figures 1.4 and 1.5. Jeon et al. presented a novel approach in their work where they used a diffractive optical element and a bare imaging sensor to achieve results which were comparable to state of the art HSI techniques [17].

In this work we present two alternative designs for a computational snapshot HSI system which make the system easier to reproduce. This system relies on compressed sensing theory to algorithmically reconstruct a 3D scene from a 2D measurement. The first design consists an off-the-shelf sensor with protective cover glass while keeping the other components of the Spectral DiffuserScope as is. The second design has the spectral filter placed right behind the diffuser with any off-the-shelf imaging sensor. We outline the fabrication and calibration

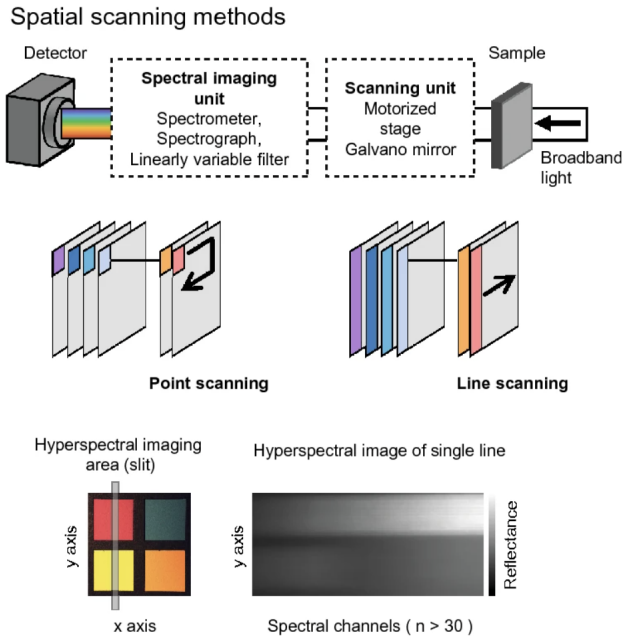

Figure 1.2: Common spatial scanning Hyperspectral Imaging (HSI) systems, figure taken from [29].

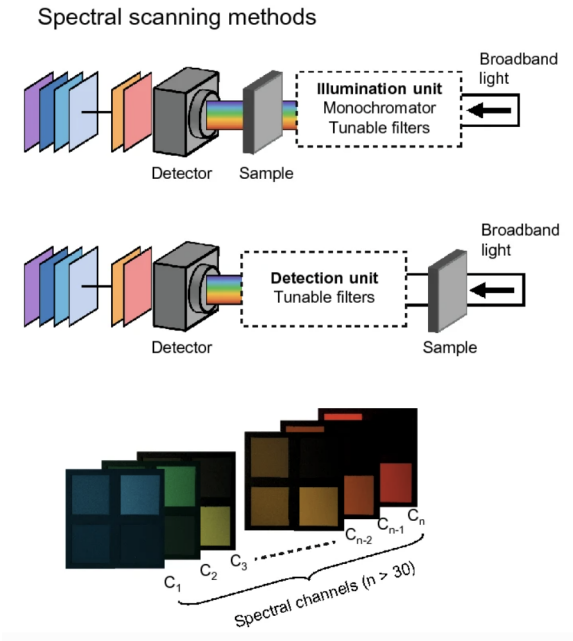

Figure 1.3: Common spectral scanning HSI systems, figure taken from [29].

procedures for both designs, show the initial results for both designs (design 1 - experimental results, design 2 - simulation results), and discuss the limitations and trade-offs associated with them.

1.2 Relevant Background

This section discusses the relevant physics and math background most relevant to this thesis.

Computational Imaging

Computational imaging is an emerging field that combines digital signal processing, optics, and image sensors to create new imaging systems with enhanced capabilities. It relies on the co-design of hardware and advanced algorithms to acquire and reconstruct images which may achieve higher resolution, higher dimensional data, and so on. Advancements in computing power have propelled this field forward resulting in widespread innovation in the field. One example of computational imaging is light field photography, which captures both the intensity and direction of light rays in a scene and allows for digital refocusing and depth

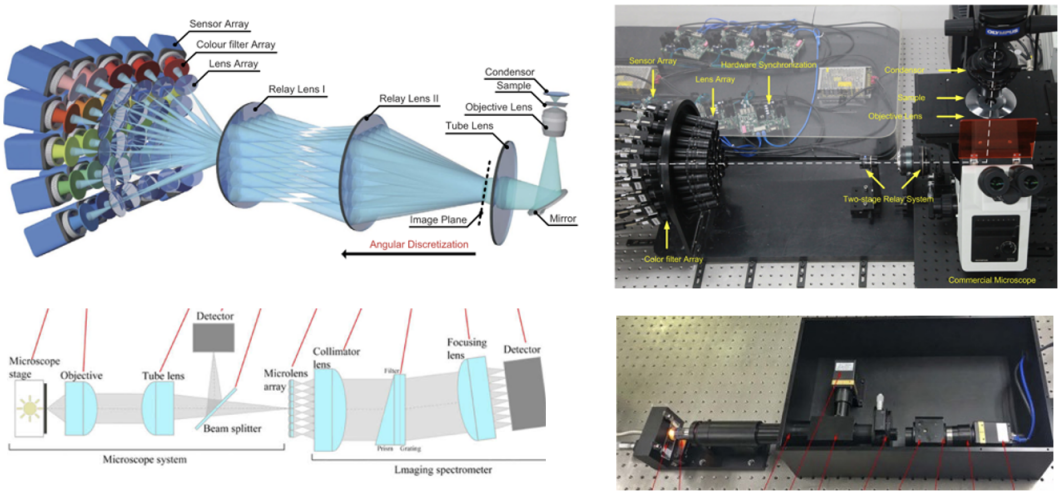

Figure 1.4: Images of a snapshot HSI system taken from [28] and [30]

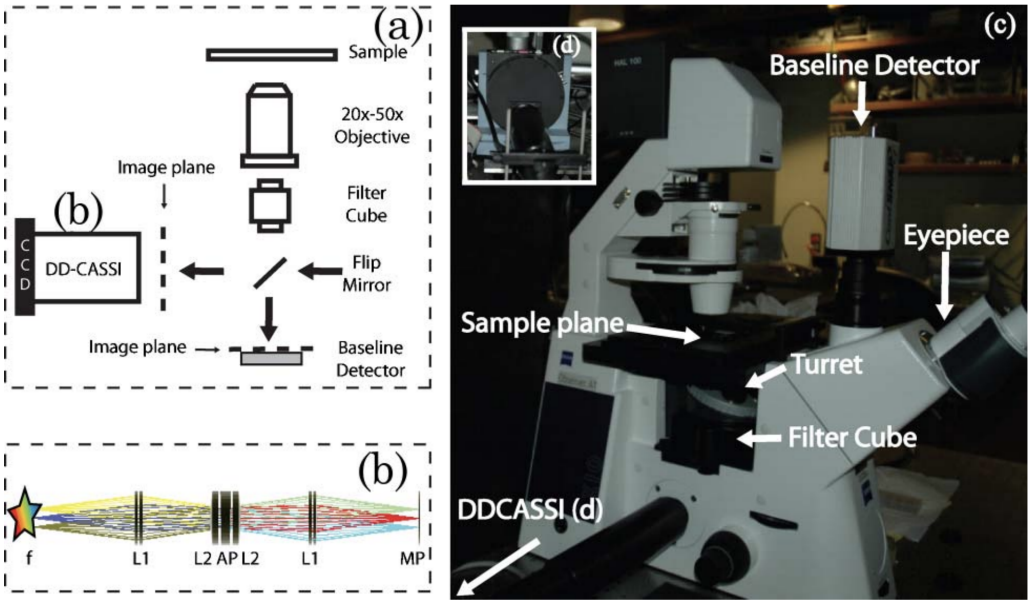

Figure 1.5: Images of a snapshot HSI system taken from [12]

estimation [24]. Compressive sensing, multi-spectral imaging, super-resolution imaging, and coded aperture imaging are some of the other important techniques in computational imaging. Mait et al. provide a detailed account of what the field is about, how it has become increasingly relevant for a variety of applications, and some of the recent advances in the field [21].

Compressed Sensing (CS)

In this section we will discuss one of the most important underlying principles for a number of computational imaging systems including the system discussed in this thesis. Compressed sensing (CS) is a signal processing technique that enables acquisition of high-quality signals with fewer measurements by exploiting the underlying structure of the signal to reconstruct it faithfully. Traditionally, acquiring a signal entails taking measurements at a high sampling rate (as per the Shannon-Nyquist sampling theorem) to guarantee that all of the information in the signal is captured. Signals, however, are often compressible, i.e., they can be represented by a limited number of non-zero coefficients in a suitable basis. We spread out the sparse information contained in the signal, this is called multiplexing. We can now sub-sample these multiplexed measurements. The measurements are then processed using advanced algorithms to recover the underlying signal with high accuracy. One of major advances in CS was in the work done by Candes et al, which showed that perfect signal recovery was guaranteed using CS given that the signal of interest is sparse in a known domain and the signal is extremely dense in the domain in which it is being measured (incoherent sensing modality) [9]. One of the key benefits of CS is that it can significantly reduce the acquisition time and/or the data storage requirements, which is particularly useful for high-speed or high-resolution imaging applications.
This technique is particularly useful in cases where the signals have some common structure. For instance, when signals have similar sparsity patterns in a certain domain, we can design a multiplexed measurement scheme to reduce the number of measurements required to faithfully reconstruct the signal [8]. This is very relevant to computational imaging applications because a number of them aim to reconstruct a high-dimensional scene from a limited number of measurements. For instance, in the case of snapshot hyperspectral imaging, we try to recover a 3D hypercube from a 2D measurement. This is an underdetermined problem, but CS theory guarantees successful recovery of the signal given that the signal is sparse and the sensing modality is incoherent.

Optimization Theory

To use CS we must multiplex our measurements and sub-sample them in the multiplexed domain. This means we have to reconstruct the scene we are imaging by solving an inverse problem - using a set of measurements to estimate the scene that would result in those measurements. The inverse problem for our system boils down to an optimization problem, which is why we need to understand the fundamentals of convex optimization.

Convex optimization theory is a mathematical framework used to solve a broad range of optimization problems in fields like signal processing [11], machine learning [7], and finance [6] to name a few. Convexity is a property of a function that means it is always "bowed" upwards, and its curvature does not change in any direction. This property ensures that the function has only one local minimum which is also the global minimum - the point where the function has its lowest value. We will be using convex optimization to reconstruct our 3D scene throughout this thesis. The problem is set up as the minimization of a function which we were call the cost function.
In practice, such inverse problems need to be solved iteratively since these problems seldom have closed form solutions. However, traditional gradient descent with a fixed step size takes long to converge. Instead we use the FISTA algorithm [5] - an iterative algorithm used for solving convex optimization problems. The FISTA algorithm is a modification of the classic iterative shrinkage-thresholding algorithm (ISTA) [13] that achieves faster convergence rates. ISTA is a first-order gradient-based algorithm that updates the solution by taking a gradient step and then applying a thresholding operation to enforce sparsity constraints [13]. The thresholding operation sets coefficients of the solution that are smaller than a given threshold to zero. The FISTA algorithm builds on ISTA by adding a momentum term that accelerates the convergence of the algorithm [5]. The momentum term allows the algorithm to take larger steps in the direction of the gradient, which can improve convergence. Additionally, FISTA uses a line search to determine the step size, which can lead to better convergence rates than fixed step sizes.

Linear Shift Invariant (LSI) Systems

We want to be able to mathematically model our imaging system to recover our hypercube algorithmically. In this section we will dicuss a class of systems that is relevant to our imaging system. Let us consider a system which takes an input signal $f[x]$ and gives an output signal $g[x]$. For any such system to be an LSI system, it must satisfy the following properties:

- Linearity: If the input is a linear combination of signals, the output is also a linear combination of outputs corresponding to those signals. If $f_1 \rightarrow g_1$, and $f_2 \rightarrow g_2$:

$$af_1[x] + bf_2[x] = ag_1[x] + bg_2[x] \tag{1.1}$$

- Shift-Invariance: A shift in the input signal shifts the output by the same amount, while maintaining the same output waveform. Mathematically, if $f_1 \rightarrow g_1$, and $f_2 = f_1(x - x_0)$:

$$f_2 \rightarrow g_2 = g_1(x - x_0) \tag{1.2}$$

LSI systems are commonly used in various applications, such as image and speech processing, communication systems, and control systems. One of the advantages of such systems is that they can be represented mathematically using the convolution operation with the impulse

response of the system. This means such systems can be completely represented by their impulse response -

$$g(x) = f(x) * h(x) \tag{1.3}$$

where g_x is the ouput, f_x is the input, h_x is the impulse response of the system, and $*$ is the convolution operator. The takeaway here is that the impulse response of a LSI system is enough to model it. This will come in handy when we try to mathematically model the elements in our imaging system.

Optical Diffuser

One of the optical components in our imaging system is the optical diffuser which helps us in multiplexing information from our scene. An optical diffuser is a device that scatters light without impacting its spectral composition. Optical diffusers are commonly used in various applications, such as photography, lighting, and display technology. There are a variety of diffusers for different applications like ground glass diffusers, holographic diffusers, and micro-lens arrays. Light shaping diffusers are the most relevant to this thesis and will be part of the HSI system that we use throughout this work. This is a class of diffusers that are designed to control the spatial distribution of light and shape the light into a desired pattern. We will be assuming linear shift invariance for our diffuser, which is a reasonable for our systems since we use weakly scattering diffusers throughout this work. Consequently, we can the model the diffuser using a convolution with its impulse reponse, which is called the Point Spread Function (PSF) of the diffuser. Intuitively, this means that the PSF moves around as we move the point source laterally and axially. This is shown visually in Figure 1.6.

Spectral Filters

Another important component of the imaging system are the spectral filters that we use for spectral sampling of the hypercube we are trying to reconstruct. There exist a wide variety of spectral filters for different kinds of applications. The spectral filters that we will be using throughout this work are narrow band spectral filters created using Fabry-Perot cavities. These filters are made up of a stack of dielectrics that act as Bragg mirrors. We obtain these spectral filter arrays from Viavi Solutions. Our filter arrays contain 8x8 tiles of different filters repeated across the entire filter array. Figure 1.7 shows the spectral response for each of the filters in the spectral filter array. Each 8×8 tile consists of 64 different narrow-band spectral filters ranging from about 380-900 nm, with an average bandwidth of () forming 64 wavelength channels which we will utilize for our HSI system discussed in the next section.

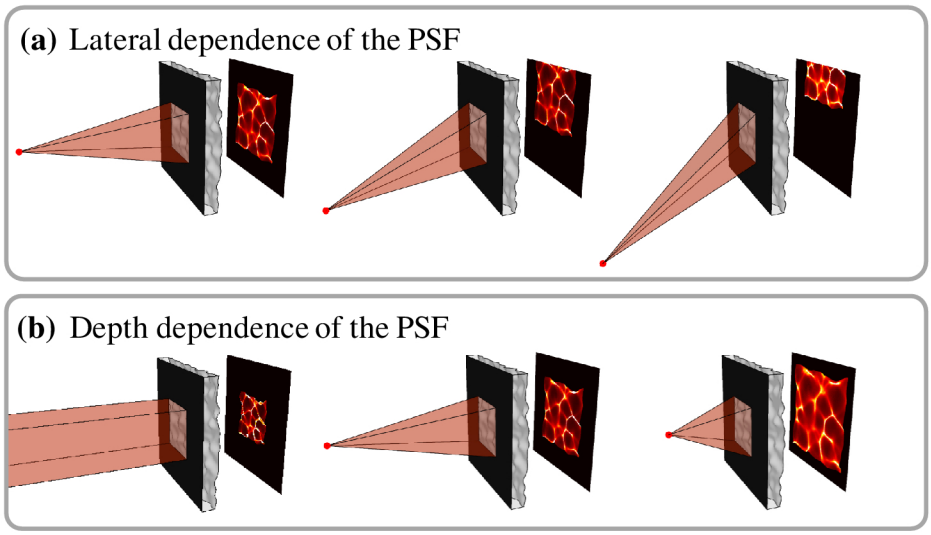

Figure 1.6: Caustic pattern shifts with lateral shifts of a point source in the scene and scales with axial shifts. (a) Ray-traced renderings of caustics as a point source moves laterally. For large shifts, part of the pattern is clipped by the sensor. (b) The caustics magnify as the source is brought closer [4].

1.3 Snapshot HSI System

This section discusses a snapshot HSI system for microscopy - the Spectral DiffuserScope, which is based on the photography version - the Spectral DiffuserCam [23] (Figure 1.8). Both systems use multiplexed measurements and compressed sensing theory to exploit the sparsity in various samples, with an optimization algorithm to reconstruct a 3D hypercube from a 2D intensity measurement. As shown in Fig. 1.9, the microscope version consists of a relay lens to relay the Fourier plane from inside the microscope, a diffuser placed in the Fourier plane, followed by a spectral filter array and an imaging sensor. Additionally, the system relies on a gradient descent based algorithm to recover the hypercube of the scene from the measurement acquired by the sensor.

Spectral DiffuserScope

In this section we will discuss the importance of each component of this system qualitatively leading to a mathematical model for this system, which is essential for the reconstruction algorithm. Before we dive into the details of the system, we first get an overarching view of how the system works. The system takes a multiplexed 2D intensity measurement on the sensor and uses compressed sensing theory to reliably recover the 3D hypercube, given that the scene in sparse in some known domain. The relay lens relays the Fourier plane

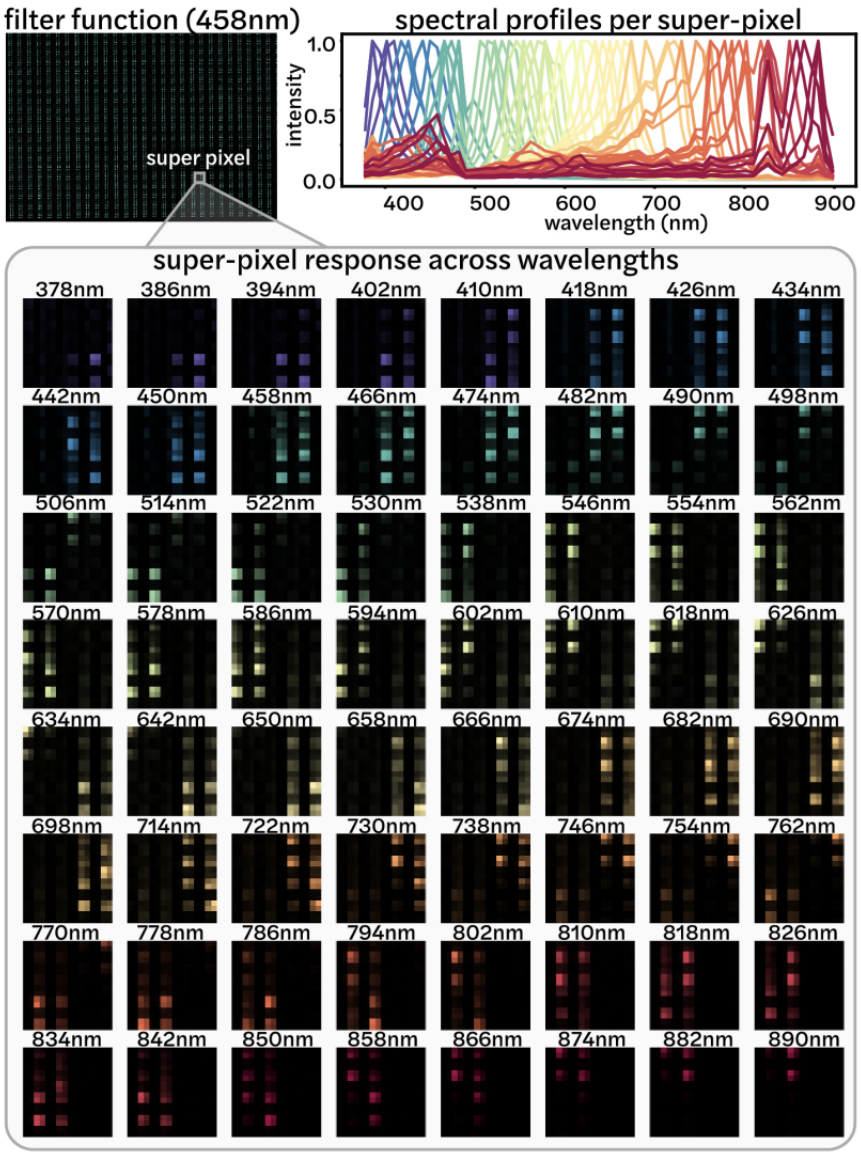

Figure 1.7: On the top left is the calibration image of the spectral filter array with a 458nm plane wave, on the top right in the spectral response for each of the filters, additionally the figure shows the response of the filter across a range of wavelengths measured using a monochromator. The super pixel refers to a single 8×8 tile on the spectral filter array. Figure taken from the paper by Monakhova et al [23].

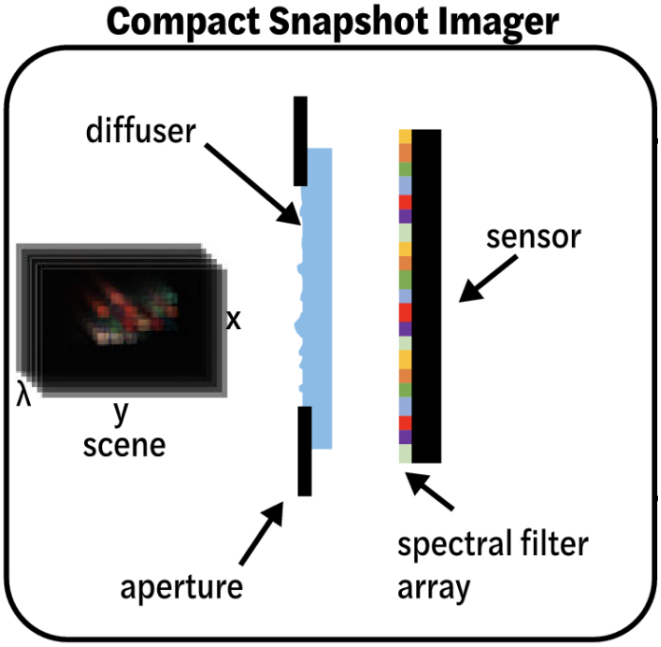

Figure 1.8: Diagram of the Spectral DiffuserCam taken from [23].

from the microscope onto the diffuser, the diffuser encodes the spatial information in our scene, and the spectral filter array encodes the spectral information in the scene. The relay lens allows us to access the Fourier plane from outside the microscope. This is followed by a diffuser which is placed in the Fourier plane of the imaging system and plays the role of the multiplexer. The diffuser maps a point in the scene to a pseudo-random pattern on the image sensor (Figure 1.6) which we call the Point Spread Function (PSF) of the diffuser. We are able to track the movement of this pattern very accurately and hence we are able to localise our point in the scene. The diffuser is followed by a spectral filter array as described earlier in the thesis.

Forward Model for the Spectral DiffuserScope

When we move a point in the scene, the caustic pattern of the diffuser moves correspondingly on the sensor, but the pattern itself remains the same, meaning that the system is linear shift-invariant. Although this is not true for all diffusers, it is a very good approximation for weakly scattering diffusers. Consequently, the light from the scene passing through the diffuser can be modeled as a 2D convolution with the diffuser's PSF (as discussed in section 1.2):

$$B_1(x, y, \lambda) = H(x, y) * V(x, y, \lambda). \tag{1.4}$$

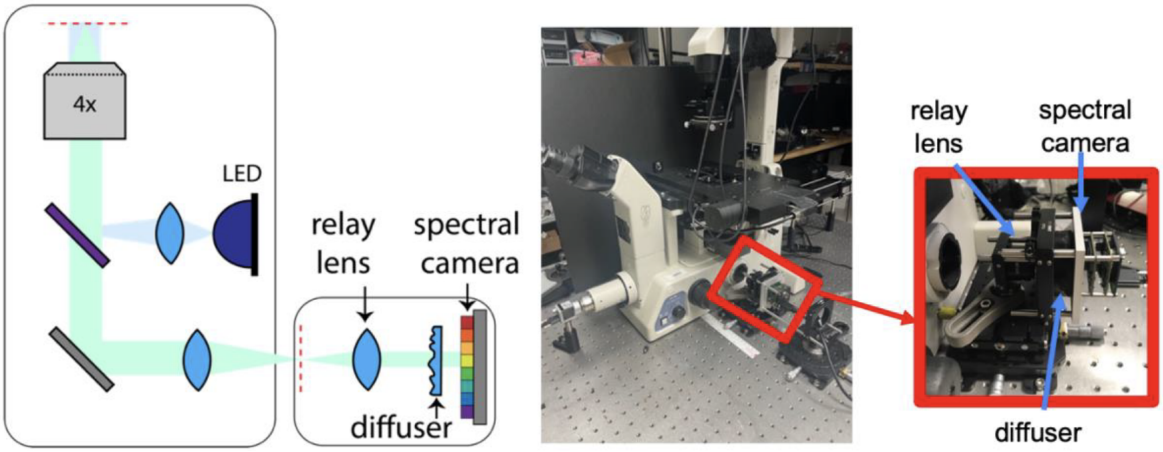

Figure 1.9: (left) The Spectral DiffuserScope microscope architecture [2], (right) image of the Spectral DiffuserScope coupled to a bench-top microscope [2].

Here, B_1 represents the intermediate measurement after the light has only passed through the diffuser, H refers to the diffuser PSF and V is the scene we are imaging. This is followed by the light passing through the spectral filter array which can be modeled by a point-wise multiplication with a 3D erasure matrix. We also add the crop function here to model the finite physical size of the sensor:

$$B_2(x, y, \lambda) = F(x, y, \lambda) \circ crop[B_1(x, y, \lambda)] = F_\lambda \circ crop[H(x, y) * V(x, y, \lambda)]. \tag{1.5}$$

Here, B_2 represents the intermediate measurement after the light has passed through the diffuser and the spectral filters and F refers to the spectral filter array matrix. However, this is not the final measurement, since the sensor captures a 2D intensity measurement where the contributions for each wavelength sum up to result in a 2D measurement. The final measurement B can be written as:

$$B(x, y) = \sum_\lambda B_2(x, y, \lambda) = \sum_\lambda F(x, y, \lambda) \circ crop[H(x, y) * V(x, y, \lambda)]. \tag{1.6}$$

Here, B refers to the final measurement on the sensor, which is a 2D intensity measurement.

Reconstruction

We use this forward model to solve an inverse problem, which in this case we do by solving an optimization problem. The optimization problem in itself is non-convex because it is an under-determined problem - has multiple possible solutions or local minima. However, we impose a native sparsity prior in our optimization problem, which helps us converge to

a unique solution. The sparsity prior effectively enforces the reconstruction algorithm to lean towards solutions which are sparse - have few non zero coefficients. This optimization problem can be expressed as:

$$\hat{V} = arg\min_{V} |B - \sum_{\lambda} F \circ crop(H * V)|_2^2 + \mu||V||_1. \tag{1.7}$$

Here $\hat{V}$ is the solution to this optimization problem - the reconstructed scene. We use the FISTA algorithm (discussed in Section 1.2) to solve the optimization problem [5].

Advantages of the Spectral DiffuserScope

This system is compact (about 6 inches long), requires only 4 additional components (relay lens, diffuser, spectral filter, image sensor), and can be coupled into existing bench-top microscopes easily. Additionally, the system decouples the spatial and spectral encoding, which allows the system to circumvent the classical spatial-spectral resolution trade-off experienced by traditional snapshot HSI systems.

Limitations of the Spectral DiffuserScope

The system requires that the spectral filter array be placed right on top on the imaging sensor. Most imaging sensors come with a cover glass, and to ensure that this system works, we must have the cover glass removed and the spectral filter array stuck right on top of the sensor. This requires a custom fabrication process for the camera, resulting in long lead times, reduced accessibility for such a system, and also introduces the possibility of the sensor getting damaged. Also, not all sensors can be obtained without a cover glass which means we are greatly limited in terms of the sensitivity of our system depending on sensors available with the cover glass removed. Another disadvantage of the system presented by Monakhova et al. is that this system requires some region of the sensor to be left empty for calibration [23]. This is not optimal as it sacrifices a part of the FOV of the system just for calibration purposes.

1.4 Outline of the Thesis

We will address the limitations discussed in the previous section throughout this thesis. The objective of this work is to present design modifications (hardware and computational) that allow this architecture to be more easily reproducible. We want the hardware to be easier and faster to fabricate, using mostly off-the-shelf components in the design. Another important issue we want to address is that we want the imaging system to be able to use any image sensor available based on the sensitivity requirement of the application, instead of being limited to special ordered sensors with their cover glass removed. Additionally, we will demonstrate calibration procedures that do not require us to sacrifice a portion of our FOV.

Here is an outline of the thesis:

Chapter 1: This chapter introduces the reader to the concept of hyperspectral imaging, what kind of HSI systems exist, the relevant background required to understand the work presented in this thesis, and the computational snapshot HSI system (Spectral DiffuserScope) on which we base our camera architecture. The working principles of the hardware and the algorithm for the Spectral DiffuserScope (a snapshot HSI system) are discussed at length. Finally, we discuss the limitations of the Spectral DiffuserScope design and how we will circumvent those limitations throughout the rest of the thesis.

Chapter 2: This chapter discusses the first design solution that we propose - placing the spectral filter on top of a sensor with a cover glass. This design is much easier to fabricate and uses off-the-shelf components allowing for any image sensor to be used. We discuss the fabrication steps and a new calibration process for the camera design, as well as the challenges introduced by the presence of a cover glass. We present experimental results to demonstrate that we can make appropriate computational modifications to make our design work.

Chapter 3: This chapter discusses an alternate design where we place the spectral filter right behind the diffuser. This design allows us to decouple the hyperspectral nature of our system from the sensor, allowing for any image sensor to be used in the design. We outline the fabrication and calibration processes for this new design and discuss the design choices associated with this new system. Furthermore, we discuss the considerations associated with this new design and future possibilities.

Chapter 4: This chapter outlines the contributions made by this work and the key takeaways from this thesis. It also outlines the future possibilities associated with this work.

Chapter 2

Imaging through the Cover Glass

2.1 Overview

One of the goals of this thesis is to demonstrate an easily reproducible version of the Spectral DiffuserScope architecture for HSI imaging. One of the major limitations presented by the Spectral DiffuserScope is that the camera requires custom fabrication to stick the spectral filter array onto the sensor with it's cover glass removed. This makes the camera much harder to reproduce due to the long lead times in getting the custom fabrication done. Instead we want to be able to use any off-the-shelf imaging sensor as part of the imaging system. This chapter discusses the how we built and tested the system with a sensor which had a cover glass (Fig. 2.1), and the experimental results we were able to achieve.

2.2 Methods

This section details the fabrication and calibration procedures for the new camera.

Fabrication of the new Camera

Material Required:

- Optical Adhesive (Norland 61)
- Imaging Sensor (BaslerCam AG daA1600-60um)
- Spectral filter array (8×8 filter array - 64 spectral channels, filter size 450um)
- Optical Diffuser (0.5-degree Luminit diffuser)

Fabrication Procedure (Figure 2.2):

1. Applied a very small amount of optical adhesive on the imaging sensor.

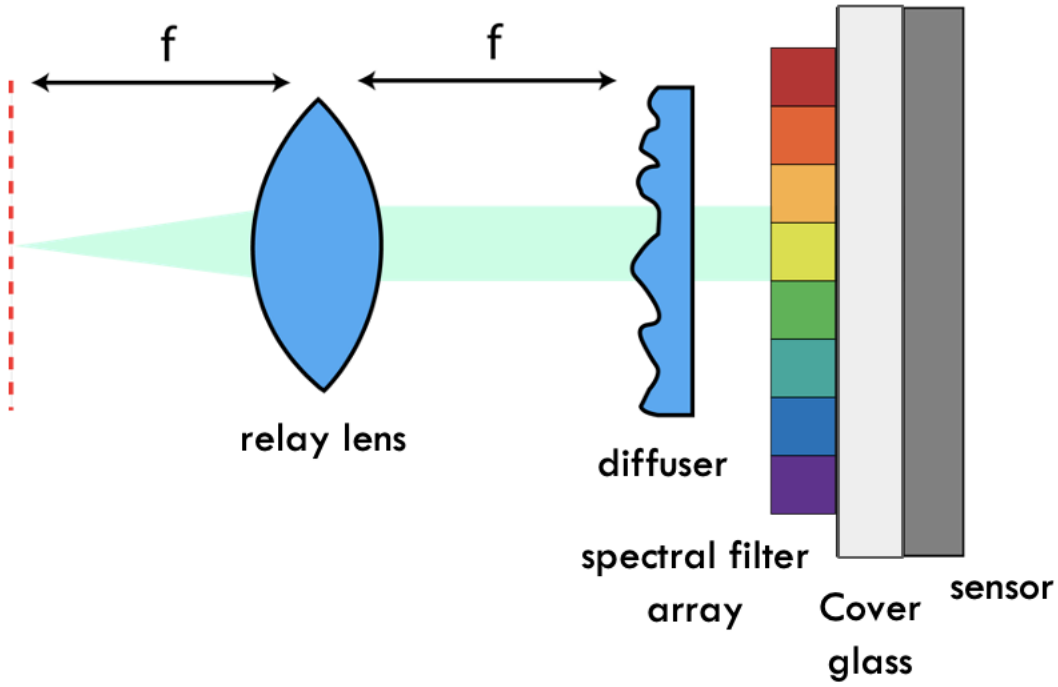

Figure 2.1: Optical diagram for the proposed design consisting of a relay lens, a diffuser, a spectral filter, and an imaging sensor (with a cover glass).

2. Carefully placed the spectral filter array onto the imaging sensor.
3. Cured the setup under UV light to allow the glue to harden.
4. Mounted the diffuser onto this setup to complete the imaging system.
5. Finally we formed an aperture on the diffuser using black tape, the aperture was sized such that the PSF is larger than a single 8x8 tile on the filter. We used a PSF which was about 20 percent larger that than a single tile on the filter.

Calibration for the new Camera

As we saw in the previous chapter, the reconstruction algorithm for our HSI system requires us to know the PSF of the diffuser and the spectral filter matrix beforehand. This means we must calibrate both of these to be able to successfully reconstruct scenes using our camera. Here we outline the calibration procedure for the aforementioned in detail.

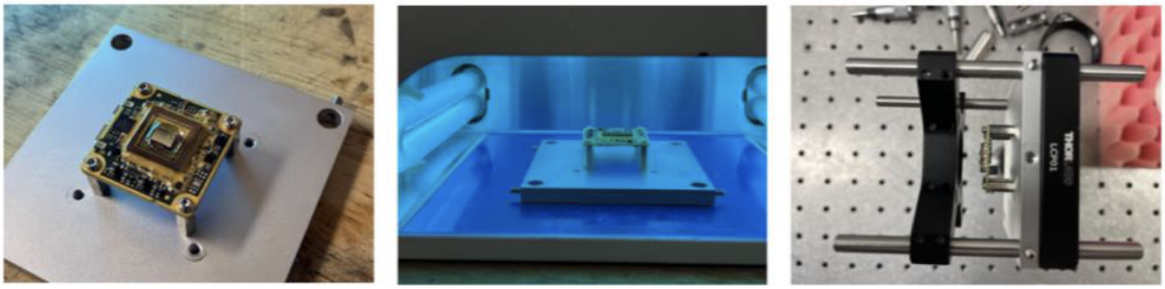

Figure 2.2: The images depict each step of the fabrication procedure: (left to right) optical adhesive was applied to the sensor, filter array was stuck on, cured under UV light, and the diffuser was mounted.

Spectral Filter Matrix Calibration

The spectral filter matrix was calibrated using a diffraction-grating monochromator (Optometrics SDMC1-03) with measurements taken from 380-880 nm uniformly spaced by 5nm. Here, calibration wavelength range depends on your choice of filters. Figure 2.3 shows the setup used for calibrating the spectral filter matrix for our imaging system. The monochromator has to be far enough from the camera such that the light incident on the camera is approximately a plane wave because the filters have an angular response. We also want uniform illumination over the entire filter array to ensure accurate calibration.

Diffuser PSF Calibration

As mentioned in the introduction, one of the disadvantages of using the previous camera with the tiny filters was that a portion of the camera had to be left uncovered by the spectral filter array to capture the PSF. This sacrifices a portion of the field-of-view (FOV). Instead, here we use a larger filter size, and capture the PSF through the filters. Using an iPhone flashlight, we took multiple measurements while translating the iPhone horizontally, used cross-correlation between consecutive measurements for point source localization (to calculate the shift between two consecutive measurements), and then the PSF was learned using a reconstruction algorithm explained later in this section (Eq. 2.1).

We use the forward model that we discussed for the Spectral DiffuserCam here (Equation 1.6), except that we have a new masking matrix to replace our filter matrix. We can make this simplification because we take multiple measurements through the spectral filters using a broadband source of light which illuminates a column of the spectral filter array that lets through parts of the visible spectrum. The forward model is fairly unchanged for a single measurement, but the difference is that we are not trying to learn the scene, we are learning the PSF, and so our unknown now is the diffuser PSF (h). Also, to make the reconstructed

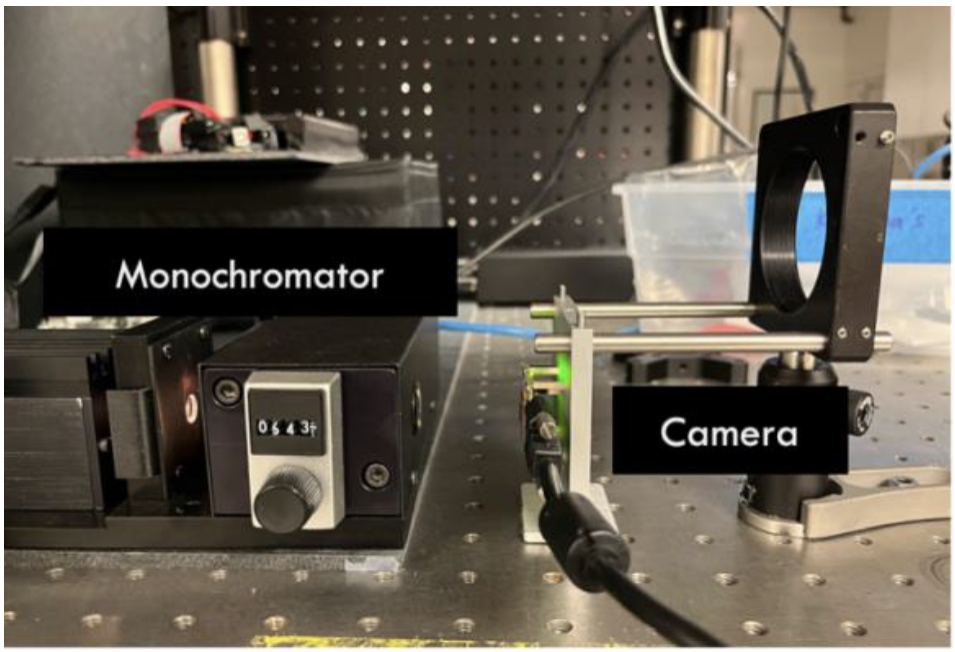

Figure 2.3: The setup used for the spectral filter calibration using a monochromator.

PSF more accurate, we used cross-correlation between successive measurements to localize our point source.

$$\hat{H} = arg\min_{H \geq 0} \sum_{n} |B - M \circ crop(H * V)|_2^2 \tag{2.1}$$

Here, B refers to the 2D measurement on the camera, M refers to the masking matrix, H refers to the diffuser PSF that we want to reconstruct, V is the scene containing the algorithmically-localized point source, and n is the number of measurements taken. The optimization problem was solved using the FISTA algorithm (discussed in Section 1.2).

2.3 Results and Discussion

Initial Experimental Results

The initial experimental setup used a programmable LED Panel with multicolored (RGB) LEDs as the object as shown in Figure 2.6. This allows us to control the scene easily, collect experimental data controllably and reliably, and also serves as a sparse scene. For the initial reconstructions, we used the forward model from before (Eq. 1.6) without modelling the cover glass in our algorithm. From the initial reconstruction results, it was clear that the spatial localization was working well for our reconstructions as can be seen in Figs. 2.7, 2.8.

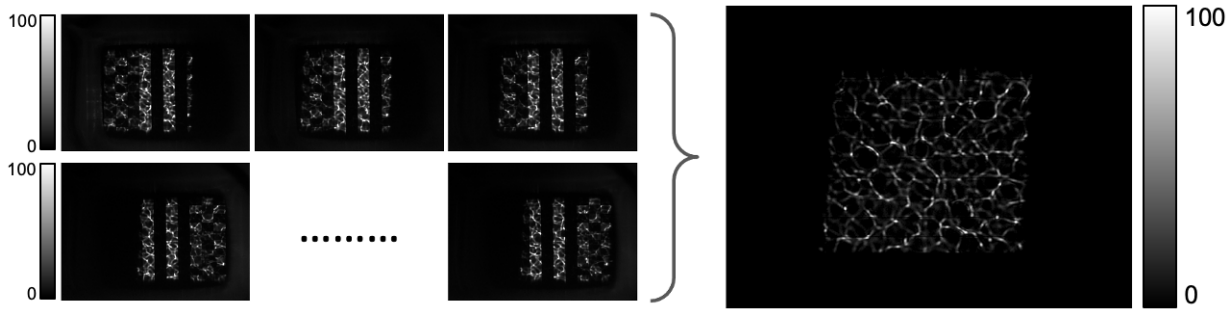

Figure 2.4: (left) These are some of the acquisitions we took for different locations of the source (iPhone flashlight), (right) The final reconstructed PSF was obtained by solving a reconstruction algorithm (Eq. 2.1) using the measurements with the source translated across the scene.

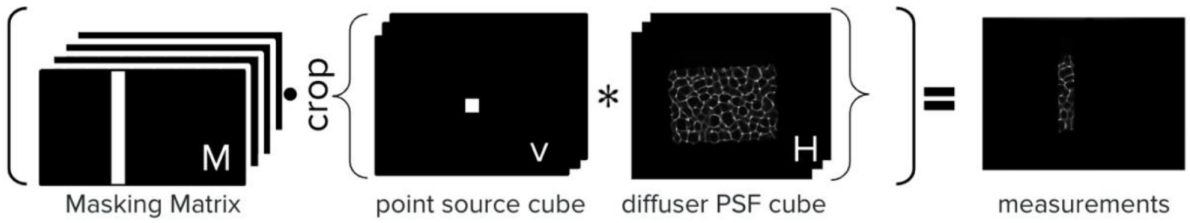

Figure 2.5: The forward model used in our reconstruction algorithm to obtain the diffuser PSF. We translate a point source across a scene and rely on this forward model to solve an inverse problem to obtain the diffuser PSF

The reconstructed spectrum also matched the ground truth spectrum with reasonably high accuracy. However, it is noteworthy that the object was located centrally in the FOV in this case.

Spectral Artifacts

Despite the encouraging initial results without making any changes to our reconstruction algorithm, we realized that we had not tested any scenes that were towards the edges of the FOV. So we tested our system by capturing images for a green LED at three positions, far left part of the FOV, center of the FOV, and far right part of the FOV. On completing the reconstructions for these 3 cases, we saw that as we moved the object to the edges of the FOV, the spatial recon still worked fine, but there was an artifact peak in the infrared region in the reconstructed spectral response (Fig. 2.9).

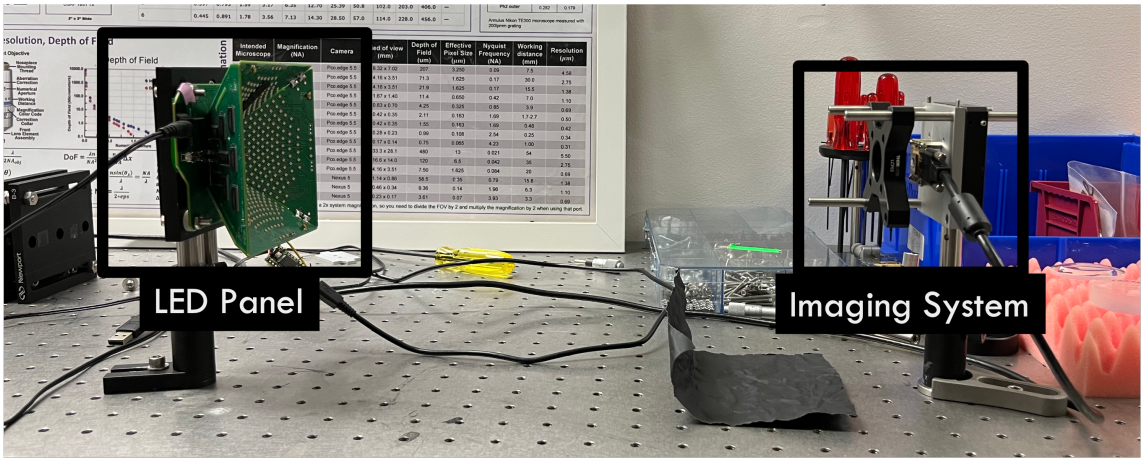

Figure 2.6: The experimental setup used for initial experiments consisted of a programmable LED panel and the HSI system.

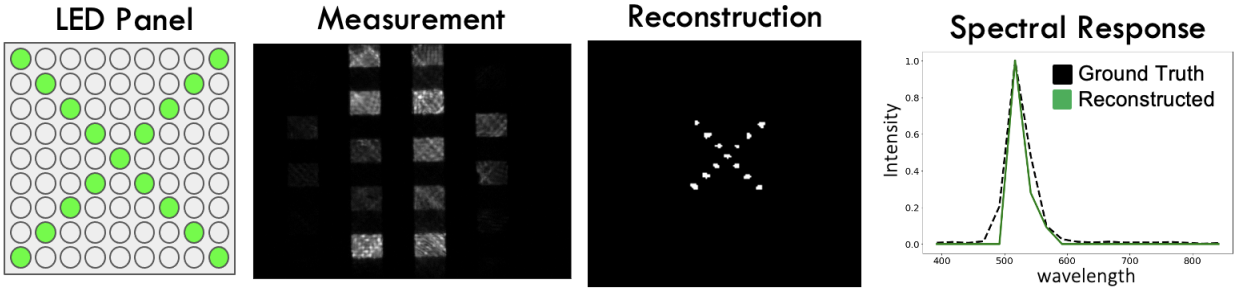

Figure 2.7: (left to right) A programmable LED panel was used as an object with an 'X' illumination pattern, the measurement as captured by the camera, xy-projection of the reconstructed 3D data cube, spectral response of the LEDs at one of the points in the reconstructed scene.

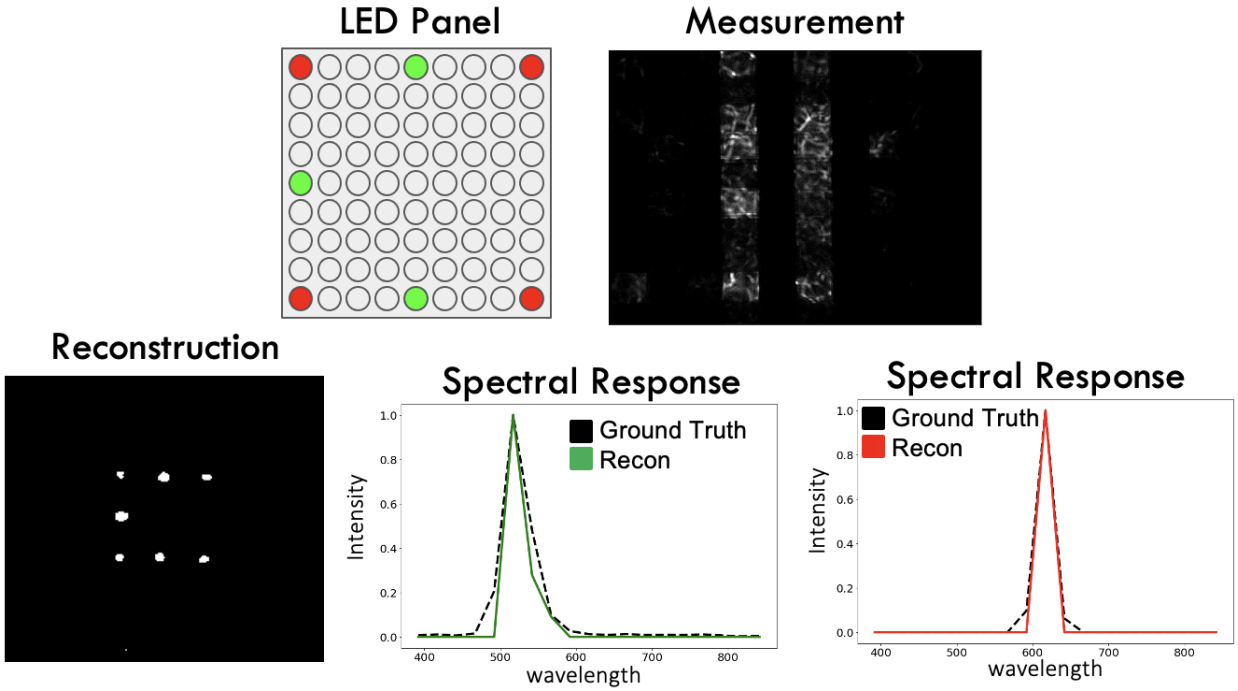

Figure 2.8: (top row: left to right) A programmable LED panel was used as an object with an 7 LEDs turned on, the measurement as captured by the camera, (bottom row: left to right) xy-projection of the reconstructed 3D data cube, spectral response of one of the green LEDs in the reconstructed scene, spectral response of one of the red LEDs in the reconstructed scene.

Understanding Crosstalk

To explain the spectral artifacts in our reconstructions as we moved our object to the edges of the FOV, we must remind ourselves that since we use an off-the-shelf image sensor, it comes with a cover glass on top of it. The cover glass introduces separation between the spectral filters and the sensor, which introduces crosstalk between the light passing through adjacent filters. Due to this separation, now our previous forward model is only approximately true. The model is still accurate for objects that are central to the FOV, however that is not the case for the edges of the FOV. Specifically, the spectral filter array cannot be modeled as a point-wise multiplication for objects at the edges of the FOV.

Fixing Reconstructions

In this section we will propose two methods to obtain faithful reconstructions using our HSI system despite the cover glass. The first of these is an unbiased approach - independent of

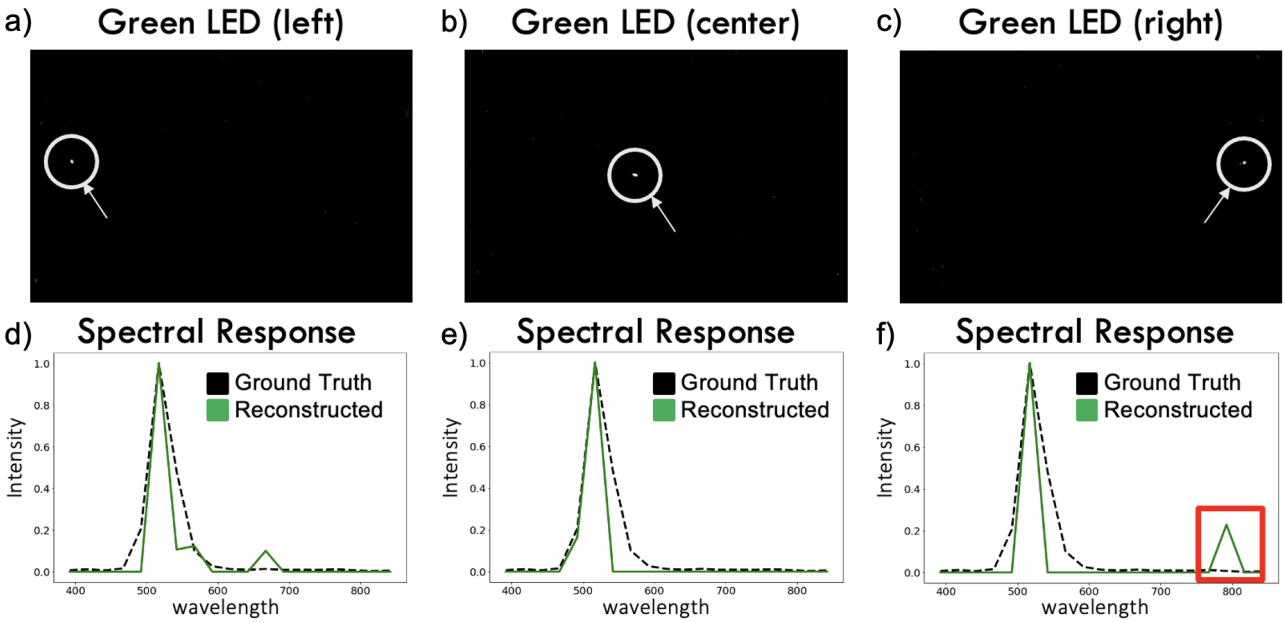

Figure 2.9: A programmable LED panel was used as an object with a single green LED illuminated, reconstructions for when the object was placed on the far-left edge of the FOV, middle of the FOV and far-right edge of the FOV, a) xy-projection of the reconstructed 3D data cube for the green LED on the left edge of FOV, d) spectral reconstruction of the LED at the point in the reconstructed scene (a) as compared to the ground truth spectrum, b) xy-projection of the reconstructed 3D data cube for the green LED in the middle of FOV, e) spectral reconstruction of the LED at the point in the reconstructed scene (b), c) xy-projection of the reconstructed 3D data cube for the green LED on the right edge of FOV, f) spectral response of the LED and the point in the reconstructed scene (c). The spectral response has 64 wavelength channels binned into 20 channels.

the sample or application. This method relies on the fact that the pixels that are most affected by the crosstalk are the ones behind the interfaces of adjacent spectral filters. Hence, we choose to ignore these pixels for the spectral reconstruction to be accurate. We used simple geometry to find what fraction of the pixels would be affected by crosstalk in our scene and selectively erased those pixels computationally (in our case it was approximately 30 percent of pixels). Using some rudimentary edge filtering and some manual intervention, we formed an erasure grid using our spectral filter matrix. Our design choice of using larger filters in our filter array meant that we were able to successfully reconstruct our scene despite applying an erasure (throwing away part of the measurement).

The second approach is an application-dependent approach. Several applications that employ hyperspectral imaging have a spectral basis, i.e., a discrete set of spectra such that any

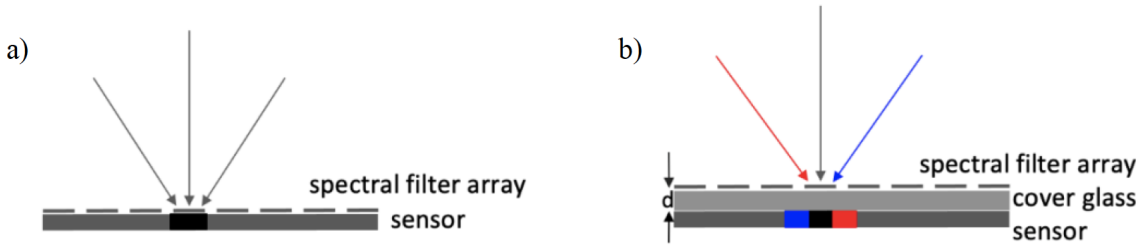

Figure 2.10: a) For the previous custom fabricated camera design, light incident onto a filter at different angles activates the same pixels on the sensor. b) For our proposed hand-fabricated camera, light incident onto a filter at different angles activates different pixels on the sensor.

observed spectral response in the scene is a combination of these basis spectra. For example, in the simple case of the LED panel we used in our experiments, all detectable spectral responses are a combination of the red, blue, and green LED spectra. In such scenarios, we use the limited possibilities of spectral responses to our advantage and create a spectral basis, D. We can impose an additional constraint in our reconstruction algorithm - that the spectral response of any point in our scene must be some linear combination of the basis spectra.

$$\hat{V} = arg\min_{V} |B - \sum_{\lambda} F \circ crop(H * V)|_2^2 + \mu||V||_1 \qquad \text{s.t.} \quad DU = V \tag{2.2}$$

Here, B refers to the 2D measurement on the camera, F refers to the spectral filter array, H refers to the diffuser PSF, V is the scene we want to reconstruct, and D is the spectral dictionary, where each column is a basis spectra. Figure 2.11 shows the impact of applying these computational modifications to the case where a single green LED is the edge of the field of view. As we can see, both these modifications resolve the spectral artifacts problem that our system was suffering from earlier, thus allowing for more faithful reconstructions.

In this section we were able to demonstrate that the system works in the photography setting for simple samples. We recommend using the spectral priors method for any application where an underlying spectral basis is known beforehand. However, we do recognize that this is not true for a number of HSI applications. The erasure grid method is applicable to a much wider range of applications. However, to use this approach for reconstructions, we must ensure that our filters are large enough so that we can throw away a part of the measurement and still reconstruct the scene faithfully.

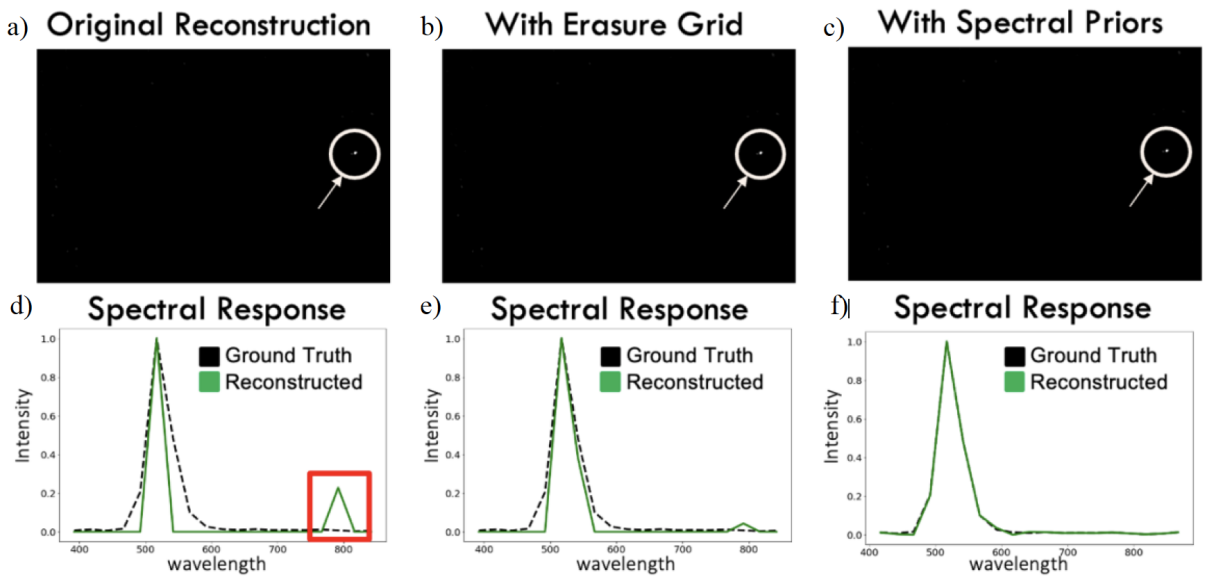

Figure 2.11: A programmable LED panel was used as an object with a single green LED illuminated, reconstructions for when the object was placed on the far-right edge of the FOV, a) xy-projection of the originally reconstructed 3D data cube, d) spectral response of the LED and the point in the reconstructed scene (a), b) xy-projection of the reconstructed 3D data cube after computationally applying the erasure grid to the measurement, e) spectral response of the LED and the point in the reconstructed scene (b), c) xy-projection of the reconstructed 3D data cube after applying spectral priors in the reconstruction algorithm, f) spectral response of the LED and the point in the reconstructed scene (c). The spectral response has 64 wavelength channels binned into 20 channels. These results show that we were able to improve spectral reconstruction fidelity by using an erasure grid and spectral priors.

Coupling with a benchtop microscope

Our next goal was to demonstrate successful reconstructions of fluorescent microscopy scenes using a sensor with a cover glass. A new system was fabricated with the procedure outlined in the first section of this chapter, and it was coupled to a benchtop microscope. This new camera used a more sensitive image sensor (IDS UI-3862LE-M imaging sensor with much longer exposure times) since we intended to use the system for fluorescence microscopy - a low-light imaging application. The spectral filter and diffuser PSF were also calibrated as outlined in section 2.2. The calibrated PSF is shown in Fig. 2.12. We saw that the reconstructed PSF had occlusions in some regions and had varying intensity across the image. This was inferior in quality to the PSF we were able to reconstruct in the photography setting, which can be explained by the illumination source we used in the microscopy setting.

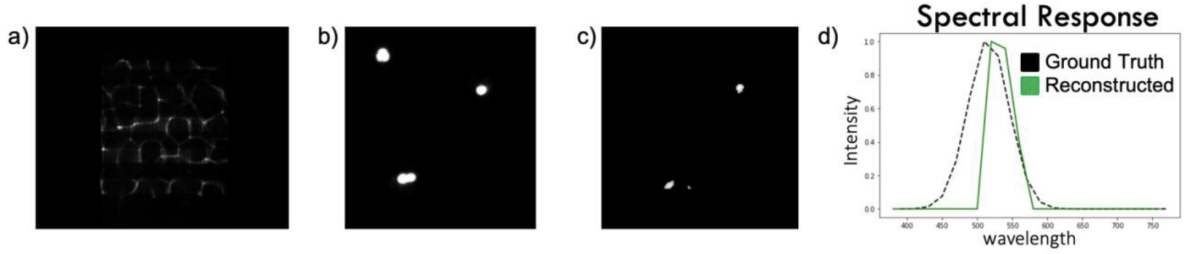

Figure 2.12: Figure 9: a) Diffuser PSF for the new camera, b) monochrome (ground truth) image of four 30um fluorescent microspheres (Fluoromax Beads by Thermo Fischer Scientific) under the microscope, c) xy projection of the reconstructed 3D data cube, d) reconstructed spectral response and the expected spectra for the green microspheres.

We used a green 5um fluorescent micro-sphere (FluoroMax Beads from Thermo Fischer Scientific) to capture the PSF. A green bead is not nearly as broadband of a source as an iPhone flashlight, hence it's masked by most of the spectral filter. Consequently, we see some occlusions in our reconstructed PSF. The poor quality of the PSF prevents us from successfully reconstructing simple fluorescence microscopy scenes. Figure 2.12 shows one of the scenes we attempted to reconstruct. The reconstructed spectrum was quite close to the expected spectral response, however the spatial reconstruction failed to recover one of the microspheres. A better calibrated PSF, without occlusions should allow us to achieve significantly better results with the same camera. To capture a better PSF, we would need to scan the point source across both x and y coordinates. This will allow us to capture the occluded parts of the PSF in these measurements which we can use to reconstruct a better PSF.

2.4 Summary

In this chapter we outlined a simple-to-fabricate design with a novel calibration procedure. We fabricated the system by hand using mostly off-the-shelf components. We demonstrated that imaging through the cover glass is indeed possible for simple sparse scenes and proposed 2 computational methods to improve the reconstruction fidelity. The next steps would be to replicate the results achieved by the Spectral DiffuserScope by coupling this system into a benchtop microscope for which we need to acquire a better PSF as outlined in the previous section. This would be followed by testing the performance of the system when imaging more complex scenes.

Chapter 3

Imaging with a wavelength-dependent PSF

3.1 Overview and Motivation

This chapter discusses an alternate design for a hyperspectral imaging system which is simple to fabricate, and much like the design discussed in chapter 2, is a slight modification of the architecture presented in the Spectral DiffuserScope paper - we simply relocate the spectral filter array from the sensor plane to the diffuser plane. The design is simple to fabricate, allows for a free choice of the imaging sensor based on the application for the imaging system, and avoids gluing a spectral filter onto the sensor which is useful for applications with expensive cameras. This design can potentially be a modular attachment that can be coupled into any imaging system to make it an HSI system. We discuss the working principles of the setup, fabrication, calibration, simulation results, and design considerations associated with this architecture.

3.2 Proposed Alternative Design

As mentioned in the previous section, the new design relocates the spectral filter array from the image sensor plane to the diffuser plane. By moving the spectral filter array to the diffuser plane we completely circumvent the custom fabrication problem presented by the initial design. Fig 3.1 shows the old and new designs side-by-side. Although the new design uses the same elements as the our previous one, operationally it is a very different system.

Forward Model

This design modification means that now we have a new forward model. We make the reasonable assumption that the diffuser behaves as a linear shift invariant (LSI) system since we will be using a weakly scattering diffuser. However, since we have now moved the spectral

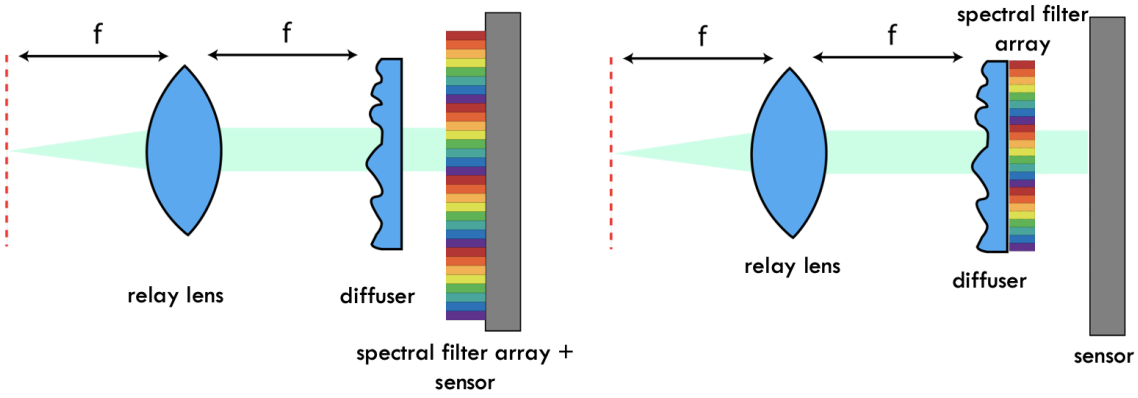

Figure 3.1: (left) Original design as introduced in chapter 1 - where the spectral filter array is adjacent to the image sensor, (right) New design proposed in chapter 3 - with the spectral filter array adjacent to the diffuser

filter array right behind the diffuser, effectively the diffuser-filter combination now has a wavelength dependent PSF. Fig. 3.2 shows an example of this wavelength dependence of the PSF at 470nm and 670nm. Mathematically we can model the diffuser-filter combination as a 2D convolution with the scene at every wavelength:

$$A(x, y, \lambda) = H_\lambda(x, y, \lambda) * V(x, y, \lambda). \tag{3.1}$$

Here, A is the measurement if the sensor size was infinite, H_λ refers to the wavelength dependent PSF, and V is the scene we are imaging. We can further understand the nature of H_λ - it is a point-wise multiplication of the spectral filter array with the diffuser PSF. In other words, the spectral filter array modifies the PSF at different wavelengths differently based on the response of the filters resulting in a wavelength dependent PSF:

$$H_\lambda(x, y, \lambda) = F(x, y, \lambda) \circ H_1(x, y). \tag{3.2}$$

Here, F refers to the spectral filter array matrix, and H_1 is the wavelength independent PSF of the diffuser. The final measurement is given by:

$$B = crop(\sum_\lambda A(x, y, \lambda)) = crop(\sum_\lambda H(x, y, \lambda) * V(x, y, \lambda)), \tag{3.3}$$

where B is the final measurement captured by the sensor.

Reconstruction

The reconstruction is very similar to what we had done for our original design. We use the forward model from the last section to solve an inverse problem to reconstruct our scene. We

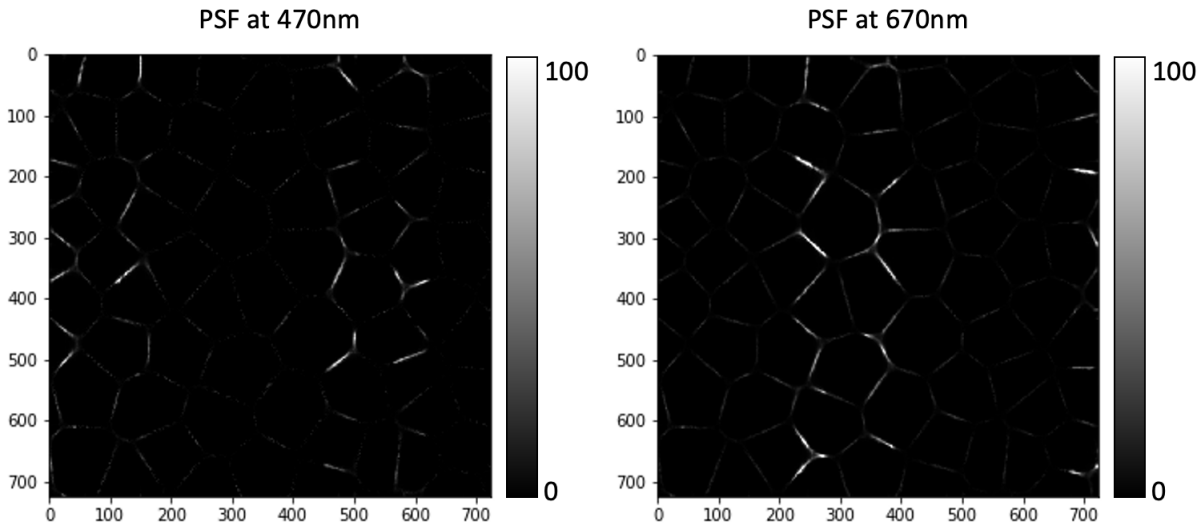

Figure 3.2: The figure shows the simulated PSF of the diffuser-filter combination at 470nm and 670nm respectively. As we can see from the images above, the PSF of the diffuser-filter combination is wavelength dependent.

rely on CS to guarantee convergence of our reconstruction algorithm to the correct solution. In practice we are solving an optimization problem which tries to minimize measurement error along with a native sparsity prior. This optimization problem can be expressed as -

$$\hat{V} = arg\min_{V} |B - crop(\sum_{\lambda} H_\lambda * V)|_2^2 + \mu||V||_1. \tag{3.4}$$

Here, $\hat{V}$ is the solution to this optimization problem, the reconstructed hypercube. We use the FISTA algorithm for faster convergence to the solution of the optimization problem.

3.3 Methods

This section briefly outlines the proposed fabrication and calibration procedures for the new design.

Fabrication

Material Required:

- Optical Adhesive (Norland 61)
- Imaging Sensor (BaslerCam AG daA1600-60um)

- Spectral filter array (8×8 filter array - 64 spectral channels, filter size **um**)
- Optical Diffuser (0.5-degree Luminit diffuser)

Fabrication Procedure (Figure 2.2):

- Apply a very small amount of optical adhesive on the smooth side of the diffuser.
- Carefully place the spectral filter array onto the glue.
- Cure the setup under UV light to allow the glue to harden.
- Add any image sensor to this setup to complete the imaging system (with appropriate sensitivity for a particular application).
- Add an aperture on the diffuser, sized such that it is larger than one 8x8 tile on the spectral filter array.

Calibration

We outlined the reconstruction algorithm for our new HSI system and to be able to successfully reconstruct images from our system we must know the wavelength dependent PSF H_λ beforehand. This camera has a simpler calibration process in that we only need a single calibration procedure since H_λ can be calibrated using a calibration setup including a monochromator. We must have a plane wave from a monochromator incident onto the setup because we are trying to capture the PSF at different wavelengths. We scan through all the wavelengths of interest and we record a different measurement at every wavelength which corresponds to the PSF at that particular wavelength. Finally we can stack all these measurements into a single matrix to form H_λ.

3.4 Simulation Results and Discussion

Before we fabricate the system, we have certain design choices to make. The most obvious design parameters associated with our new architecture are the filter size and the density of our PSF. It is a non-trivial problem to determine how the system performance would change as we modify these parameters. This section discusses the initial simulations we performed to understand what choice for these design parameters would be optimal for the imaging system. For these simulations, PSFs of 3 different densities (90um, 150um, and 300um average pattern diameter) were used - as shown in Figure 3.3. We tested each of these PSFs with 2 different filter sizes - as shown in Figure 3.4. The objects used for the simulations were a sparse scene containing multi-colored beads spelling out CAL and a multi-colored USAF Target. The USAF target is a resolution test chart which consists of numerous small target shapes exhibiting a stepping through a range of precise spatial frequency specimens. The same objects were used across all 6 simulations to perform an apples-to-apples comparison

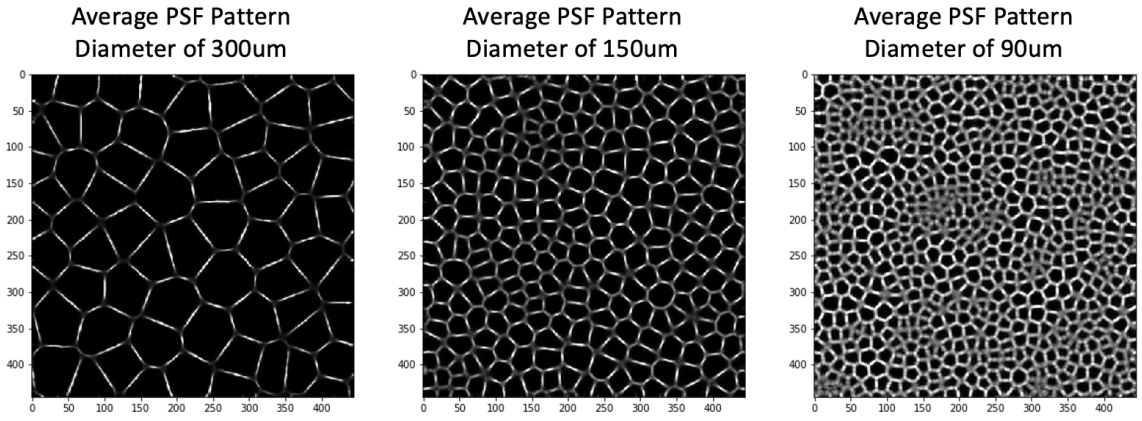

Figure 3.3: (left to right) The images show simulated PSFs of increasing feature densities with average pattern diameters of 90um, 150um, and 300um.

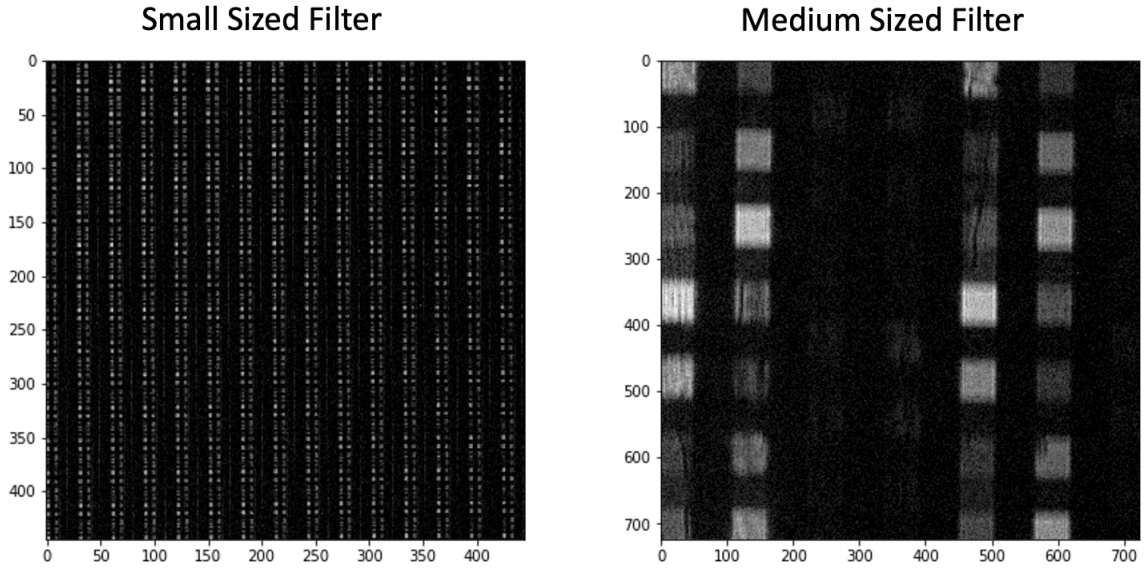

Figure 3.4: (left) Calibration image for the smaller filters at 430nm. (right) Calibration image for medium filters at 445nm.

for different choices of the filter size and PSF. When characterizing the imaging system, we primarily care about two important metrics, the spatial reconstruction fidelity of the system and the spectral reconstruction fidelity of the system.

First, let's discuss the spatial reconstruction fidelity of the system. The results from our initial simulations are shown in Figs. 3.5 and 3.6. The initial results seem to indicate that using the smaller filters results in sharper reconstructions. This is clearly visible in the zoomed in images in the second and fourth columns of Figs. 3.5 and 3.6. However, the choice of PSF feature density is not as clear from the results. The most dense PSF, which has an average pattern diameter of 90um, seems to be performing worse for both filter sizes. However, there is not enough to decisively choose one PSF from the 150um and 300um pattern diameters. The zoomed-in images look slightly sharper for the 300um PSF but the difference is subtle. Overall, the simulation results seem to be pointing us towards a smaller filter size and a fairly large feature size for our PSF to get good spatial reconstructions. However, these results are not conclusive and must be investigated further as these simulations have no noise added in.

Next we look at the the spectral reconstructions in Figures 3.7 and 3.8. This figure shows the reconstructed spectrum for one of the points in the scene. As the figure reveals, the reconstructed spectral response using the medium filters was closer to the actual spectrum for both the CAL beads and the USAF target. This conclusion is further backed by the fact that the wavelength-dependent PSF has a much higher auto-correlation than cross-correlation with PSFs at other wavelengths. Figure 3.9 shows the maximum correlation value for the 90um PSF at 580nm when correlated with the PSf at 40 different wavelength channels for both the medium and small filters. We want this peak to be as sharp as possible which is why the secondary peak that appears in the plot for the small filters is highly undesirable. Unfortunately, the results are not conclusive in indicating which PSF density would be preferable for better spectral fidelity but the reconstructions look slightly better for the 300um PSF.

The optimal design parameters for this HSI system are unclear as we saw through this section. This is left as an open problem for the reader with the note that our analysis does suggest that the choice of the filter size and PSF density will not be absolute because depending on whether a particular application requires better spatial or spectral accuracy the optimal design may vary. Another degree of freedom which we have not explored in our system is the the filter design, i.e. the location of each individual spectral filter in the array. This is another design parameter that we can play around with to potentially obtain better results

This design relies on a wavelength-dependent PSF for HSI, which is similar, in principle, to the approach used in the work presented by Jeon et al. [17]. The system they presented contains a diffractive optical element to generate a PSF that rotates as the wavelength on

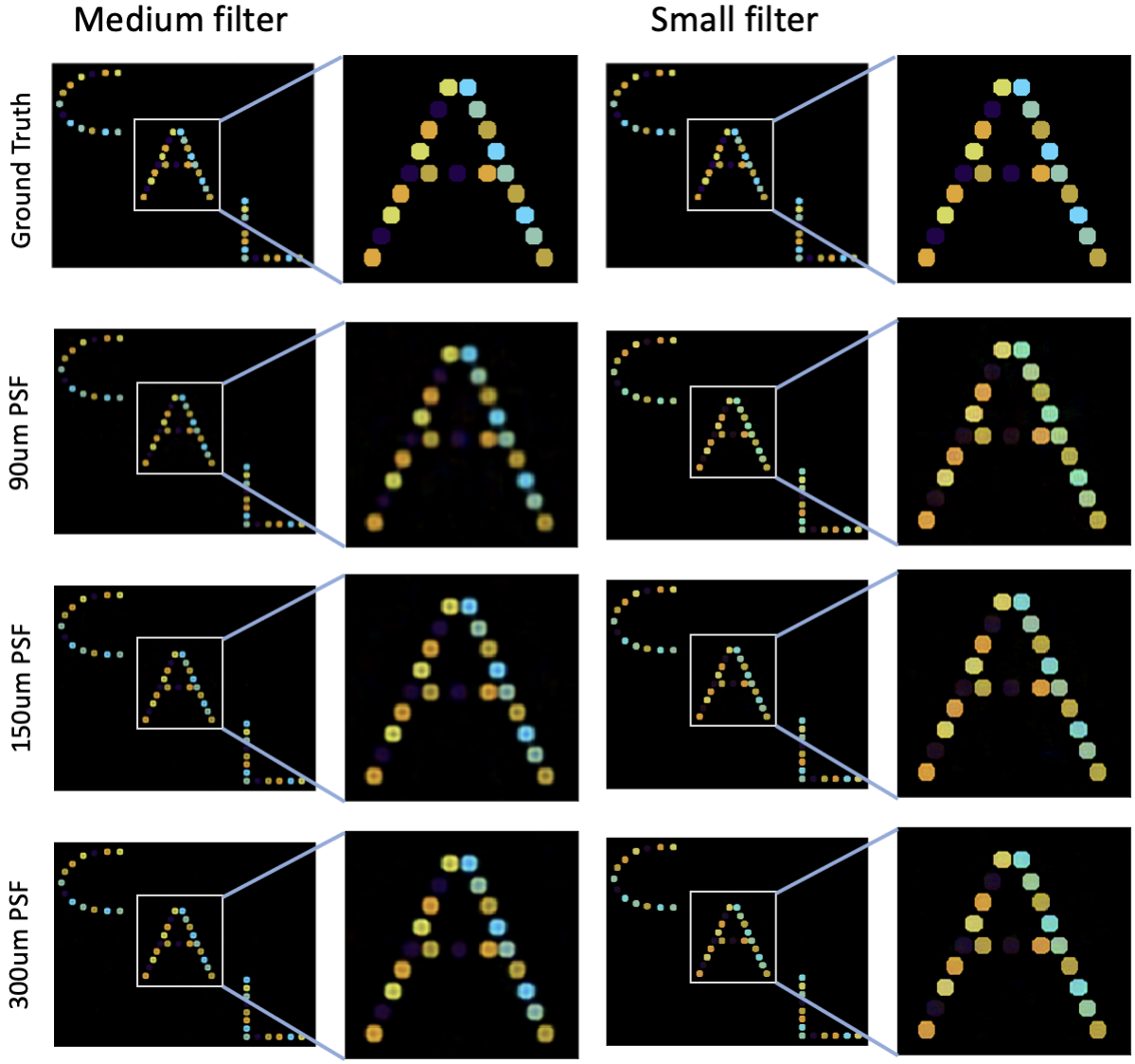

Figure 3.5: The figure shows a comparative table of CAL beads reconstructions with different filters and PSFs. The first row shows the object itself, the second, third, and fourth row show the reconstructions for PSFs with average pattern diameter of 90um, 150um, and 300um respectively. The first column corresponds to the results for the medium sized filter and the second column shows a zoomed in portion of the reconstructions. The third column corresponds to the results for the small sized filter and the fourth column shows a zoomed in portion of those reconstructions. The results indicate that in a noise-free simulation, the smaller filters have sharper spatial reconstructions, however, there is no obvious trend with regards to PSF density.

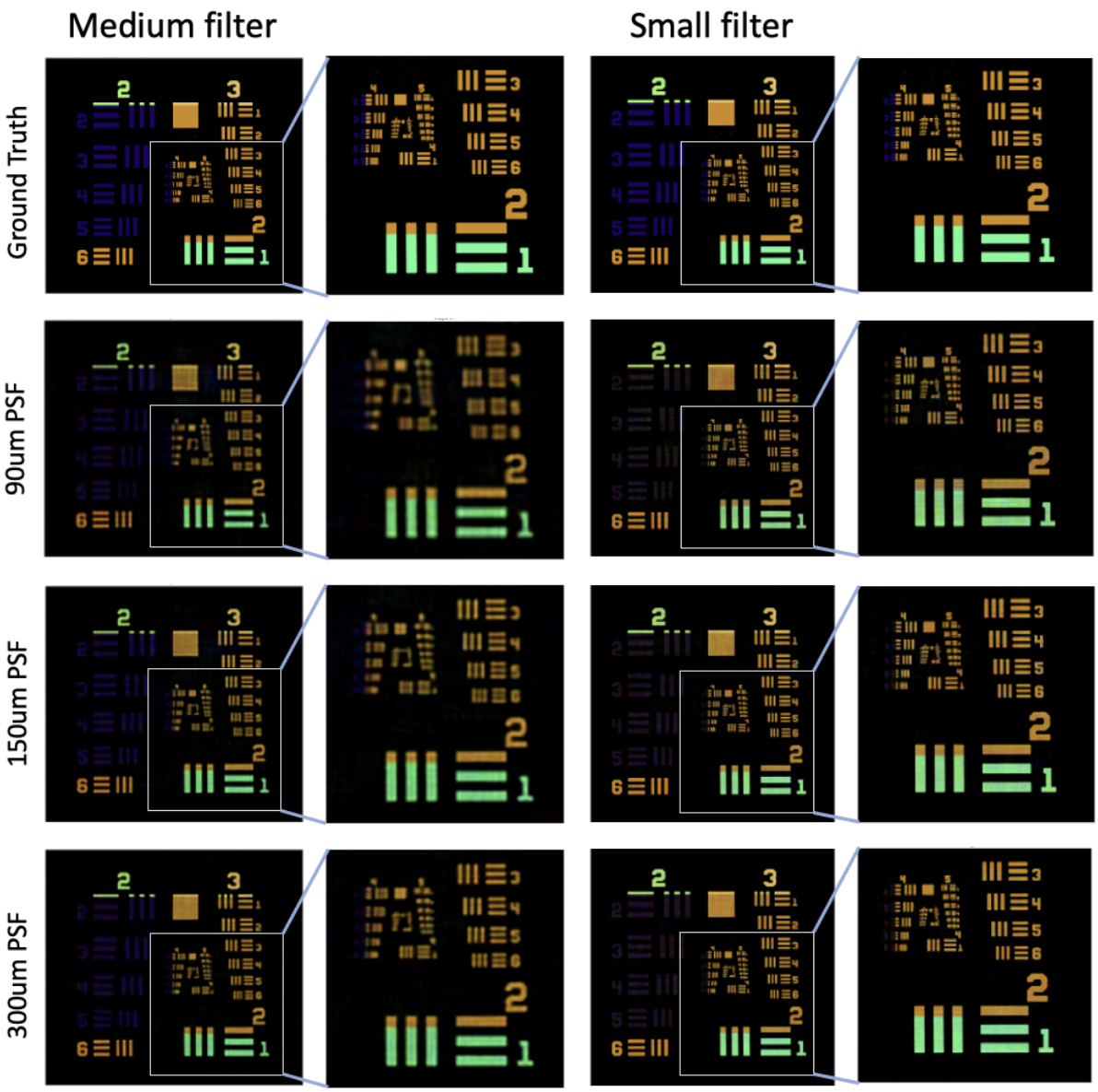

Figure 3.6: The figure shows a comparative table of USAF target reconstructions with different filters and PSFs. The first row shows the object itself, the second, third, and fourth row show the reconstructions for PSFs with average pattern diameter of 90um, 150um, and 300um respectively. The first column corresponds to the results for the medium sized filter and the second column shows a zoomed in portion of the reconstructions. The third column corresponds to the results for the small sized filter and the fourth column shows a zoomed in portion of those reconstructions. The results indicate that in a noise-free simulation, the smaller filters have sharper spatial reconstructions, however, there is no obvious trend with regards to PSF density.

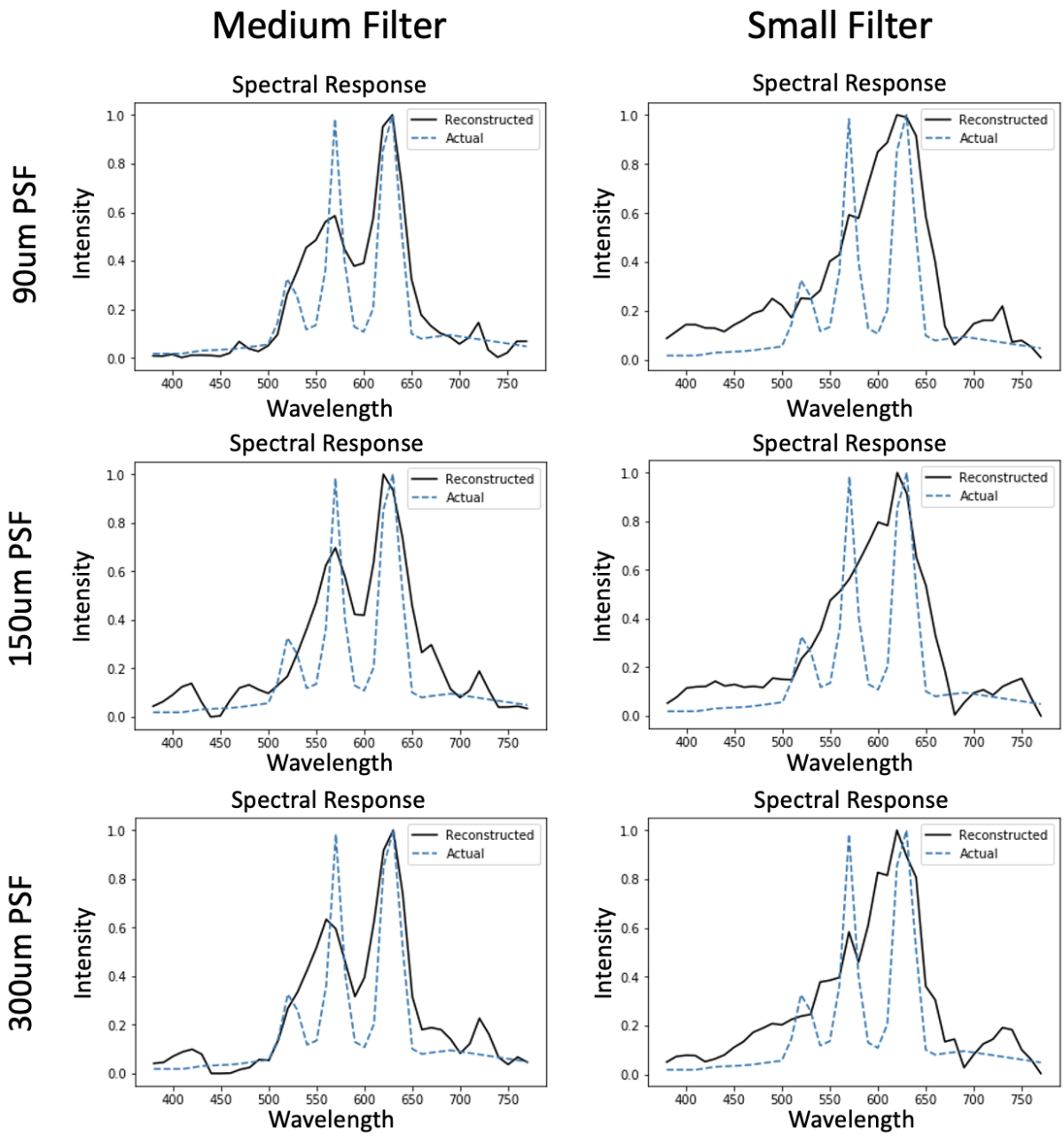

Figure 3.7: The figure shows a comparative table of the spectral response of one of the points in the CAL beads reconstruction for different filters and PSFs. The first, second, and third row show the spectral responses for PSFs with average pattern diameter of 90um, 150um, and 300um respectively. The first column corresponds to the results for the medium sized filter and the third column corresponds to the results for the small sized filter.

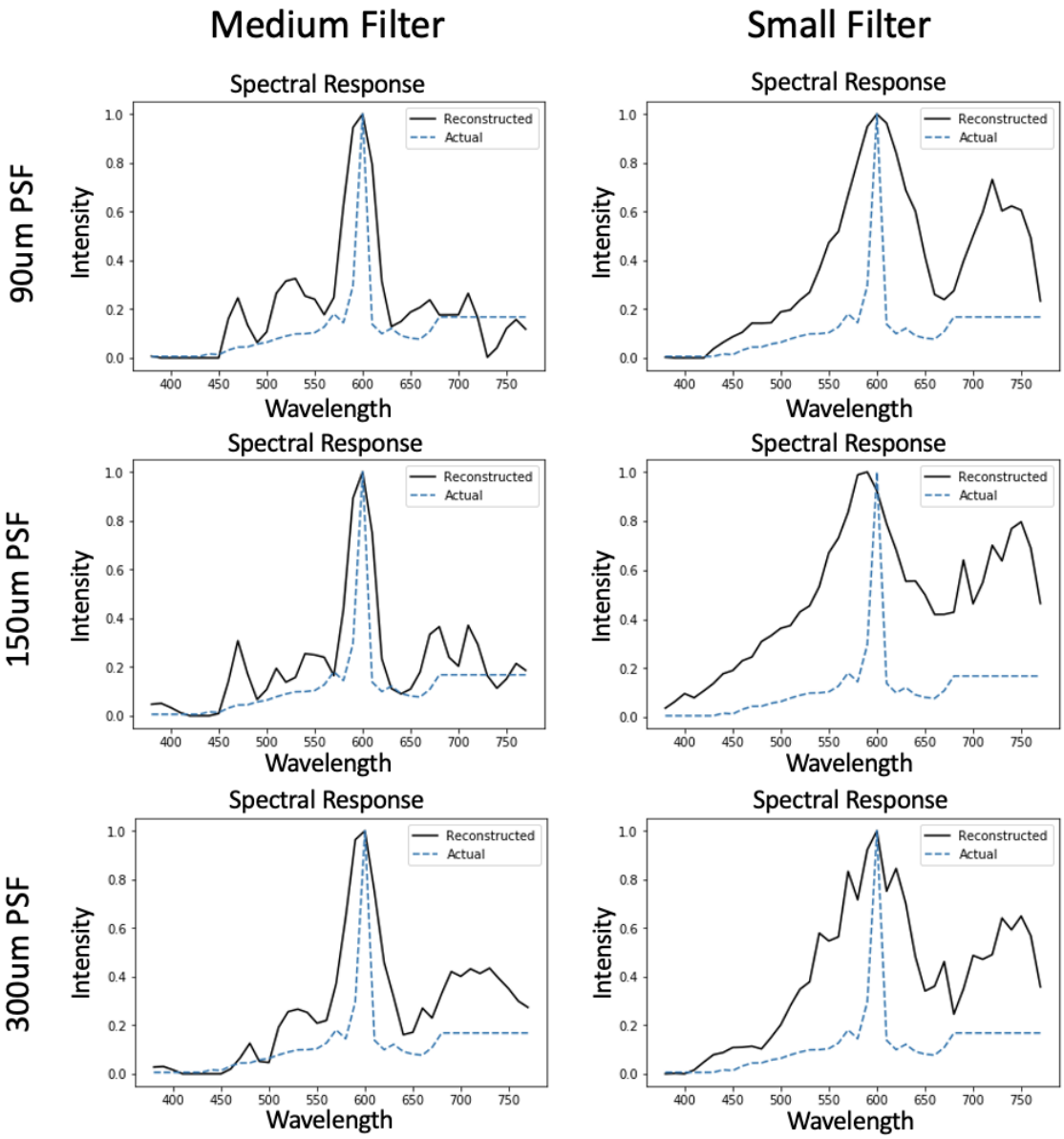

Figure 3.8: The figure shows a comparative table of the spectral response of one of the points in the USAF target reconstruction for different filters and PSFs. The first, second, and third row show the spectral responses for PSFs with average pattern diameter of 90um, 150um, and 300um respectively. The first column corresponds to the results for the medium sized filter and the third column corresponds to the results for the small sized filter.

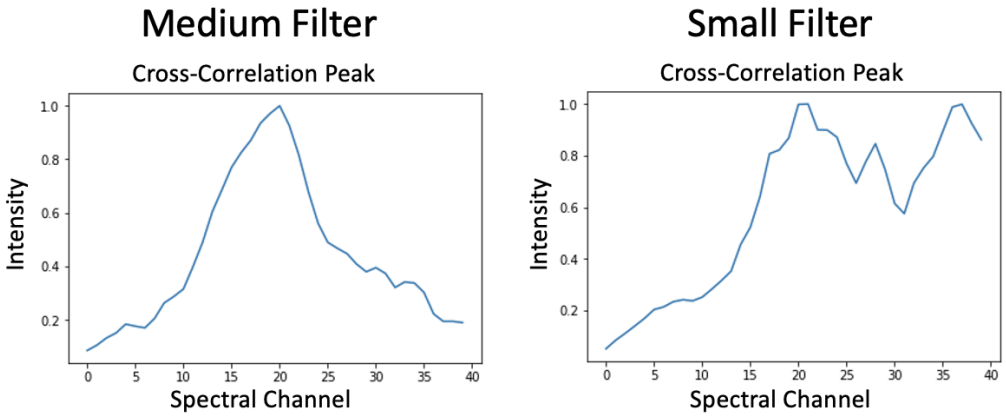

Figure 3.9: Plots of the maximum correlation value for the 90um PSF at the 20th wavelength channel when correlated with the PSF at 40 different wavelength channels for both the medium and small filters

incident light changes. However, they use learned methods for reconstructing their scene unlike the iterative approach we have presented in this work. It would be interesting to see how using learned reconstruction algorithms would modify our results. Another challenge with the system presented by Jeon et al. is they use a diffractive optical element in their system which requires a comprehensive custom fabrication process. On the contrary, the design we presented is very simple to fabricate, requiring an off-the-shelf optical diffuser and a spectral filter array of your choice. Our design also allows for a much simpler way to choose the spectral bands of interest, by simply modifying the spectral filters used in the filter array. Regardless, the promising results demonstrated by Jeon et al. are certainly encouraging for further pursuing this design.

3.5 Summary

This chapter talks about an alternative design where the spectral filter is placed right behind the diffuser to create a wavelength dependent PSF which helps us recover a 3D hypercube from a 2D measurement. We propose a fabrication and calibration scheme for this new design. Furthermore, we discuss how the filter size and the feature density of the PSF affect system performance and show initial simulation results to better our understanding of the tradeoffs associated with the system. Finally we talk about the work from another group which also uses a wavelength dependent PSF for HSI and briefly compare and contrast the the two approaches. The simulation results indicate that this might be a design approach worth pursuing which is further backed up by the promising results demonstrated by Jeon et al [17]. Before fabricating the system, we encourage the reader to first consider the application

for the system. This should help decide the spectral and spatial resolution requirements for the system, which can then inform the choices for the filter size, PSF density, and also the design of the filter itself (location of individual filters on the filter array).

Chapter 4

Conclusions

In this work, we discussed a compact snapshot HSI system - the Spectral DiffuserScope, and made modifications to the system to make it easier to reproduce. We presented 2 new designs that simplify the fabrication process for the imaging system. Both designs avoid custom fabrication steps and use mostly off-the-shelf components.

The first of these designs uses the same architecture as the Spectral DiffuserScope, but allows one to freely choose any off-the-shelf sensor for the design. We outline a simple fabrication procedure for the camera and propose a novel calibration procedure. The primary challenge with this design was to resolve the crosstalk introduced by the protective cover glass on the imaging sensor. However, we successfully demonstrated that with simple computational modifications we can improve the reconstruction fidelity of the system for simple scenes. The first of these modifications was an application independent approach - we used an erasure grid to selectively erase the pixels at the edges of the interfaces between adjacent filters. We recognize that these pixels are the most vulnerable to crosstalk so we decide to discard them. The second modification is to impose spectral priors in the reconstruction algorithm. This approach is limited to applications where a spectral basis is known for the scenes we are imaging. Both these approaches have use-cases and allow us to successfully image through the cover glass. The system was finally coupled into a benchtop microscope and initial results from the microscope system were also briefly discussed. The next steps for this system are to get a better calibrated PSF and attempt to replicate the results that the Spectral DiffuserScope was able to achieve.

The second design that we proposed modifies the architecture so that now the spectral filter array is placed right behind the diffuser. This system is also allows us to use any off-the-shelf imaging sensor, in fact it avoids gluing on the filter to the imaging sensor which is particularly useful for applications using expensive imaging sensors. The diffuser-filter attachment is a modular component that can be coupled with any imaging sensor to give it hyperspectral imaging capabilities. We present a simple fabrication and calibration procedure for this new design. Furthermore, we discuss initial simulation results and the important design tradeoffs

associated with this architecture. The filter size and PSF density are the 2 design parameters that we can feasibly control, and the simulations indicate that the optimal design would be application dependant, specifically, whether a particular application requires higher spatial or spectral resolution. We don't claim a particular design to be optimal and that optimization is left as an open problem for future work. This design has the potential to be a very compact, modular, and flexible and warrants further development.

Bibliography

[1] Telmo Adão et al. "Hyperspectral imaging: A review on UAV-based sensors, data processing and applications for agriculture and forestry". In: *Remote sensing* 9.11 (2017), p. 1110.

[2] Neerja Aggarwal et al. "Spectral DiffuserScope: Compact Hyperspectral Imager Attachment For Fluorescence Microscopy". Focus on Microscopy. 2023.

[3] Hamed Akbari et al. "Hyperspectral imaging and quantitative analysis for prostate cancer detection". In: *Journal of biomedical optics* 17.7 (2012), pp. 076005–076005.

[4] Nick Antipa et al. "DiffuserCam: lensless single-exposure 3D imaging". In: *Optica* 5.1 (2018), pp. 1–9.

[5] Amir Beck and Marc Teboulle. "A fast iterative shrinkage-thresholding algorithm for linear inverse problems". In: *SIAM journal on imaging sciences* 2.1 (2009), pp. 183–202.

[6] Stephen Boyd, Stephen P Boyd, and Lieven Vandenberghe. *Convex optimization*. Cambridge university press, 2004.

[7] Sébastien Bubeck. "Theory of convex optimization for machine learning". In: *arXiv preprint arXiv:1405.4980* 15 (2014).

[8] Emmanuel Candes and Justin Romberg. "Sparsity and incoherence in compressive sampling". In: *Inverse problems* 23.3 (2007), p. 969.

[9] Emmanuel J Candès and Michael B Wakin. "An introduction to compressive sampling". In: *IEEE signal processing magazine* 25.2 (2008), pp. 21–30.

[10] Kun Chen et al. "Excitation spectral microscopy for highly multiplexed fluorescence imaging and quantitative biosensing". In: *Light: Science & Applications* 10.1 (2021), p. 97.

[11] Chong-Yung Chi, Wei-Chiang Li, and Chia-Hsiang Lin. *Convex optimization for signal processing and communications: from fundamentals to applications*. CRC press, 2017.

[12] Christy Fernandez Cull et al. "Identification of fluorescent beads using a coded aperture snapshot spectral imager." In: *Appl Opt* 49.10 (2010), B59–B70.

[13] Ingrid Daubechies, Michel Defrise, and Christine De Mol. "An iterative thresholding algorithm for linear inverse problems with a sparsity constraint". In: *Communications on Pure and Applied Mathematics: A Journal Issued by the Courant Institute of Mathematical Sciences* 57.11 (2004), pp. 1413–1457.

[14] Rachel E Gerver et al. "Programmable microfluidic synthesis of spectrally encoded microspheres". In: *Lab on a Chip* 12.22 (2012), pp. 4716–4723.

[15] Alexander FH Goetz. "Three decades of hyperspectral remote sensing of the Earth: A personal view". In: *Remote sensing of environment* 113 (2009), S5–S16.

[16] Hui Huang, Li Liu, and Michael O Ngadi. "Recent developments in hyperspectral imaging for assessment of food quality and safety". In: *Sensors* 14.4 (2014), pp. 7248–7276.

[17] Daniel S Jeon et al. "Compact snapshot hyperspectral imaging with diffracted rotation". In: (2019).

[18] Haida Liang. "Advances in multispectral and hyperspectral imaging for archaeology and art conservation". In: *Applied Physics A* 106 (2012), pp. 309–323.

[19] Bing Lu et al. "Recent advances of hyperspectral imaging technology and applications in agriculture". In: *Remote Sensing* 12.16 (2020), p. 2659.

[20] Guolan Lu and Baowei Fei. "Medical hyperspectral imaging: a review". In: *Journal of biomedical optics* 19.1 (2014), pp. 010901–010901.

[21] Joseph N Mait, Gary W Euliss, and Ravindra A Athale. "Computational imaging". In: *Advances in Optics and Photonics* 10.2 (2018), pp. 409–483.

[22] Dimitris G Manolakis, Ronald B Lockwood, and Thomas W Cooley. *Hyperspectral imaging remote sensing: physics, sensors, and algorithms*. Cambridge University Press, 2016.

[23] Kristina Monakhova et al. "Spectral DiffuserCam: lensless snapshot hyperspectral imaging with a spectral filter array". In: *Optica* 7.10 (2020), pp. 1298–1307.

[24] Ren Ng et al. "Light field photography with a hand-held plenoptic camera". PhD thesis. Stanford University, 2005.

[25] Huy Q Nguyen et al. "Programmable microfluidic synthesis of over one thousand uniquely identifiable spectral codes". In: *Advanced optical materials* 5.3 (2017), p. 1600548.

[26] Sima Peyghambari and Yun Zhang. "Hyperspectral remote sensing in lithological mapping, mineral exploration, and environmental geology: an updated review". In: *Journal of Applied Remote Sensing* 15.3 (2021), pp. 031501–031501.

[27] Mary B Stuart, Andrew JS McGonigle, and Jon R Willmott. "Hyperspectral imaging in environmental monitoring: A review of recent developments and technological advances in compact field deployable systems". In: *Sensors* 19.14 (2019), p. 3071.

[28] Jiamin Wu et al. "Snapshot hyperspectral volumetric microscopy". In: *Scientific reports* 6.1 (2016), pp. 1–10.

[29] Jonghee Yoon. "Hyperspectral imaging for clinical applications". In: *BioChip Journal* 16.1 (2022), pp. 1–12.

[30] Changben Yu et al. "Research on spectral reconstruction algorithm for snapshot microlens array micro-hyperspectral imaging system". In: *Optics Express* 29.17 (2021), pp. 26713–26723.